NE Atlantic continental slope stability from a numerical modeling perspective

Bellwald, B.[1,2*], Urlaub, M.[3], Hjelstuen, B.O.[1], Sejrup, H.P.[1], Sørensen, M.B.[1], Forsberg, C.F.[4], Vanneste, M.[4]

[1]Department of Earth Science, University of Bergen, Bergen, Norway

[2]Now at: Volcanic Basin Petroleum Research (VBPR) AS, Oslo, Norway

[3]GEOMAR Helmholtz Centre for Ocean Research Kiel, Kiel, Germany

[4]Norwegian Geotechnical Institute (NGI), Oslo, Norway

*benjamin@vbpr.no

Abstract

Trough mouth fans are environments characterized by high sediment supply during glacial stages and the occurrence of large-scale instabilities. The geological record indicates that several of these environments have failed repeatedly resulting in large submarine landslides. The roles of sedimentation rate, weak layers, glacial loading and unloading as well as seismic activity on triggering megaslides in trough-mouth-fan systems is still unclear. A better understanding of the preconditioning factors, triggers and consequences of these landslides is crucial due to the hazard they pose to coastal communities and offshore industries.

In this paper, we focus on the North Sea Trough Mouth Fan, which is the result of massive glacial sediment input delivered to the shelf edge through the Norwegian Channel, southeast Nordic Seas margin. The Tampen Slide, one of several large paleo-landslides that have happened within the North Sea Trough Mouth Fan, took place at c. 130 ka (end of MIS 6), and removed an estimated 1800 km^3 of sediment.

Here, we use boundary conditions from the Tampen Slide and 2D Finite Element Modeling (Abaqus software from Simulia) to evaluate the effects of variations in sedimentation rates as well as sediment properties on the generation of excess pore pressure, fluid flow, and slope stability along the axis of the trough-mouth-fan system. The model domain, 40 km in length and 2 km in height, is dominated by glacigenic debris flows and glacimarine sediment deposits. We use geotechnical data measured on samples of glacigenic and glacimarine sediment deposits from the nearby Ormen Lange gas field area to constrain the model. We evaluate the stability of the slope under various scenarios, including constant sediment loading, episodic changes in sedimentation rates and abrupt pulses in sediment delivery for a 61 kyr period (MIS 6). The models show that increased sedimentation rates during glacial stages do not generate sufficient excess pore pressure to set off a landslide. Furthermore, the simulated overpressures for the different sedimentation scenarios do not significantly differ at the end of the model runs. The results also highlight the importance of a basal glacimarine sediment layer underneath the rapidly-deposited sediments for the build-up of overpressure. Consequently, this glacimarine sediment layer has the inherited potential to act as a weak layer facilitating instability. However, as overpressure due to

sediment deposition alone does not result in slope failure, we couple the preconditioned slope with earthquake ground shaking. Based on attenuation models, an earthquake of approximately M6.9 or larger at a short distance from the Tampen Slide headwall could have triggered the landslide. Therefore, we suggest glacial sedimentation and a glacimarine sediment layer to represent preconditioning factors, and seismic shaking as the final trigger mechanism for the Tampen Slide, i.e. similar to the situation that lead to the development of the Storegga Slide in the same area.

Keywords: North Sea Trough Mouth Fan – Tampen Slide – Slope stability – Overpressure – Trigger mechanism – Earthquake – Quaternary – Glaciation – North Atlantic – Glacial geomorphology

1. Introduction

Evidence of submarine landslides is found both on low-latitude unglaciated and high-latitude (formerly) glacial-dominated continental margins (e.g. Canals et al., 2004). The largest submarine landslides, e.g. the Storegga Slide, tend to occur on continental slopes with remarkably low gradients (<2°). Despite this low dip, the remobilized slide masses runout over distances of several hundreds of kilometers (Hampton et al., 1996). Submarine landslides often develop as retrogressive translational failures, characterized by bedding-parallel glide planes that are separated by distinct escarpments (Hampton et al., 1996; Masson et al., 2010). The gravitational load and generation of overpressure linked to the rapid deposition of glacigenic debris flows (GDFs), plumite deposits and (glaci-)marine sediments seems to play a significant role for the initiation of large submarine landslides on glaciated margins (Bryn et al., 2005; Tripsanas et al., 2008; L'Heureux et al., 2013). Differences in the strength behavior of marine clays and glacial clays are a key aspect for the development of these failures (Kvalstad et al., 2005b).

Due to their potential for seafloor infrastructure damage and tsunami generation, submarine landslides may have a significant socio-economic impact (e.g. Pope et al., 2017). High sedimentation rates, changing sea levels, gas hydrate dissociation and earthquake shaking are frequently discussed as processes that affect slope stability in the submarine environment (e.g. Leynaud et al., 2009). The pre-conditioning and trigger mechanisms are, however, not always easy to establish (Masson et al., 2010). It is, however, essential for geohazard and risk assessments to understand and distinguish between preconditioning factors and factors that trigger slope failure, as well as understanding the potential consequences. Overpressure is generally considered as a key aspect in most – if not all – pre-conditioning factors (Vanneste et al., 2014).

Sediment accumulation can outpace the dissipation of pore fluids if rates are high and/or permeability is low. Overpressure, here defined as pore pressure in excess of hydrostatic pressure, reduces the effective stress in the sediments. Overpressure can exist in deep and shallow formations and it most likely occurs where fine-grained sediments having low-permeability ($<10^{-16}$ m^2) inhibit pore fluid migration or at locations affected by large forcing mechanisms, such as rapid sediment deposition (Swarbrick and Osborne, 1998; Flemings et al., 2008; Scheider et al., 2009; Dugan and Sheahan, 2012).

Large-scale slope failures have happened in regions where sedimentation rates are high (McAdoo et al., 2000; Urgeles and Camerlenghi, 2013). Having an important role in the pre-conditioning of subaquatic slopes, rapid sedimentation can set the conditions for the occurrence and volumes of large submarine mass movements (Masson et al., 2006; Dugan and Sheahan, 2012; Stoecklin et al., 2017). Numerical modeling indicates that rapid and prolonged sediment delivery from rivers or ice streams can generate sufficient overpressure to directly cause failure of nearly flat slopes (Stoecklin et al., 2017), or weaken the slope to such an extent that a moderate earthquake can cause failure (Stigall and Dugan, 2010). Overpressure generated by the rapid loading of glacial deposits during short periods of peak glaciations on top of marine sediments is likely one of the main preconditioning factors for the Storegga Slide (Fig. 1) (Berg et al., 2005), and overpressure remnants are still observed behind its upper headwall (Strout and Tjelta, 2005). Oozes underlying Pleistocene glacial sediments have been suggested to affect lateral fluid migration (Bryn et al., 2005). In order to predict the amount of overpressure that can be generated by sediment deposition over time, i.e. during consolidation, information about sedimentation rates as well as the compressibility and permeability of the sediments and how these parameters change with increasing overburden stress and compaction is required (Urlaub et al., 2012; Kvalstad et al., 2005a).

So-called weak layers are often considered to host the slip facilitating translational failure at all scales (Locat et al., 2014). Examples are the Storegga Slide (Bryn et al., 2005; Solheim et al., 2005), the intermediate-sized Cap Blanc Slide (Urlaub et al., 2018) or the much smaller Finneidfjord Slide (Vanneste et al., 2012). In this study, we define a weak layer as any geological layer or a sequence of layers promoting slope instability. Trough mouth fans (TMFs) are depositional systems characteristic for high-latitude (formerly) glacial continental margins. TMFs are largely built up by (stacked) GDFs that were deposited in periods when ice streams reached the shelf edge (King et al., 1996; Laberg and Vorren, 1996; Elverhøi et al., 1997). There is ample evidence of the occurrence of submarine landslides in these TMFs (King et al., 1996; Vorren et al., 1998; Sejrup et al., 2005; Nygård et al., 2005; Hjelstuen et al., 2007; Rebesco et al., 2013), and TMFs are excellent records to study the relationship between large submarine landslides and ice-sheet changes on different types of margins (Vorren and Laberg, 1997; Pope et al., 2018). The seafloor typically dips less than 3° in TMF areas (Gales et al., 2018).

Furthermore, seismicity in TMFs was most likely higher shortly after the deglaciation due to glacio-isostatic rebound (Byrkjeland et al., 2000; Owen et al., 2007; Lee, 2009). Following the suggestion of Hjelstuen et al. (2007), megaslides are here defined as mass transport deposits with volumes larger than 1000 km^3.

In this study, we model the stability of the slope across the North Sea TMF (Fig. 1) during Pleistocene climate changes, focusing on the effect of rapid sediment deposition and seismic shaking. This type of modeling has previously not been published on TMF systems and has the potential to contribute to identify controlling factors of slope stability on the North Atlantic margin, where the volumes involved in submarine landslides are one or several orders of magnitude higher than their counterparts on active margins (e.g. Hühnerbach et al., 2004; Urgeles and Camerlenghi, 2013). The study presented herein addresses the following questions: (1) Can increased sedimentation rates at the North Sea TMF during a period with shelf edge glaciation generate sufficient overpressure on a ~1° slope to cause slope failure?, (2) What is the effect of a glacimarine sediment layer at the base of rapidly deposited GDFs on slope stability?, (3) How important is the sedimentation pattern during the glacial period on slope stability?, and (4) What earthquake magnitude is required to trigger megaslides on a slope preconditioned by glacial sediment? Given some uncertainties in sediment parameters, as is often the case for submarine slope stability assessments (Vanneste et al., 2014), we emphasize that the results of our study should be interpreted in a qualitative rather than quantitative way.

2. Geological setting

The Pleistocene North Sea TMF lies at the outlet of the Norwegian Channel on the northern North Sea Margin (Fig. 1). Spreading over an area of 110,000 km^2 and built up by nearly 40,000 km^3 of sediments (Sejrup et al., 1996; King et al., 1996; Nygård et al., 2005; Hjelstuen et al., 2012), it is the largest Pleistocene TMF along the Norwegian continental margin (Fig. 1). The North Sea TMF is located in a region which has experienced subsidence rates of 0.7-0.8 m/kyr during the mid- and late-Quaternary (Sejrup et al., 2004). The fan has mainly been fed by erosional products delivered to the upper continental slope by the fast-flowing Norwegian Channel Ice Stream during maximum Pleistocene

glaciations in Marine Isotope Stages (MIS) 2, 6, 8, 10, and probably 12 (Fig. 3) (Sejrup et al., 2003; Nygård et al., 2005). The sediments deposited in the early Quaternary (2.6-0.8 Ma), however, are sourced from the Norwegian mainland in the east (Batchelor et al., 2017). The shelf geometry northeast of the North Sea TMF is uniform over a c. 150 km long distance, with a width of c. 60 km.

The volcanic Møre Marginal High (Fig. 2) divides the wedge-shaped North Sea TMF into two main provinces, a proximal fan province characterized by an alteration between deposits of GDFs, glacimarine sedimentation and slide escarpments and deposits, and a distal fan province dominated by slide debrites (Nygård et al., 2005). The Pleistocene sedimentary column within the proximal province has been divided into ten sequences (P1-P10) (Fig. 2) (King et al., 1996; Nygård et al., 2005), reflecting the change in the sedimentary processes through glacial-interglacial cycles. Sequences P1, P4, P5, P8 and P10 are dominated by GDFs, identified as acoustically transparent stacked lobate lenses in the acoustic data (Sejrup et al., 1996; King et al., 1998; Nygård et al., 2002). The glacimarine sediments (P2 and P6) drape the GDFs and have an acoustically laminated seismic facies, which is only visible where the sediment package is thick enough. These glacimarine deposits are characterized as more fine-grained sediments with lower unit weights and shear strengths, and higher water contents, void ratios, permeabilities, consolidation coefficients, compressibilities, plasticity and sensitivity values compared to the GDFs (King et al., 1998; Berg et al., 2005; L'Heureux et al., 2013; Llopart et al., 2014).

The three slide debrites (P3, P7 and P9) identified in the North Sea TMF are characterized by an acoustically chaotic facies between a smooth lower and irregular upper surfaces. The Tampen Slide (Figs. 1, 2), one of numerous prominent megaslides along the Norwegian-Barents Sea continental margin (e.g. King et al., 1996; Solheim et al., 2005; Hjelstuen et al., 2007), is the most recent submarine landslide initiated at the North Sea TMF. It is suggested to be of late MIS 6 age (~130 ka, Nygård et al., 2007). It has been suggested that MIS 6 was characterized by at least three shelf edge ice sheet oscillations (Fig. 3) (Nygård et al., 2005). The debrite of the Tampen Slide (P3 in Fig. 2) has been traced from c. 500 m water depth at the shelf break to more than 2000 m water depth some 200 km basin-ward, and its ~300 m-high headwall is located c. 10 km west of the shelf break (Fig. 2). Nygård et al. (2005)

154 estimated a sediment volume of 1400 km^3 failing along a 0.2-0.7°, and locally steeper (1°), slope for the
155 Tampen Slide.

156 Additional to the ~130 ka old Tampen Slide, the North Sea TMF experienced megaslides during MIS 9
157 (Møre Slide) and MIS 11-12 (Stad Slide; Fig. 3) (Nygård et al., 2005; Solheim et al., 2005; Hjelstuen
158 and Grinde, 2016). The TMF did not fail during the last glacial-interglacial cycle; however, the ~8100
159 cal. yrs BP Storegga Slide happened nearby (Figs. 1, 2) (Bryn et al., 2005; Haflidason et al., 2005;
160 calibration curve from published articles). These megaslides affect different areas of the North Sea TMF
161 (Hjelstuen et al., 2007), as the Pleistocene ice-stream patterns have changed and sediment sources varied
162 (Batchelor et al., 2017).

163 In the study area, average sedimentation rates are in the order of c. 1 m/kyr for the glacial and deglacial
164 periods (Lekens et al., 2005; Nygård et al., 2007), whereas the rates during interglacials fall in the range
165 of 0.05-0.10 m/ka, i.e. only a fraction of the rate documented for glacial periods (Haflidason et al., 1998).
166 Locally higher sedimentation rates of up to 36 m/ka are estimated near the Storegga Slide headwall
167 during the last deglaciation (Hjelstuen et al., 2004). The excess load of rapidly-deposited glacial
168 sediments and the disappearing ice sheets are suggested to have enhanced the local stress field and, in
169 turn, the seismic activity in the region (Byrkjeland et al., 2000).

170

171 ## 3. Model configuration and slope stability analysis
172

173 In this study, we use the Finite Element Modeling software ABAQUS (6.13-1) from Simulia to test
174 various hypotheses to describe the potential for slope failure in the entire model domain at any time
175 during deposition. We therefore perform a fully-coupled fluid flow-stress analysis using a model setup
176 that accounts for large displacements using the finite strain theory.

177 ### 3.1 Model setup and input parameters

178 The Finite Element 2D Model input is partly based on the continental slope setting in the area of the
179 Tampen Slide headwall including seismic reflection data interpreted by Nygård et al. (2005) (Fig. 2).
180 The model domain has been subdivided into four simplified discrete Model Units (MU) (Fig. 4; Tab. 1).

181 The seismic sequences P6-P10 (Figs. 2, 4) are summarized as "fill" material and represent MU4. We
182 consider that MU4 is in stress equilibrium, assuming that the MIS 9 Møre Slide released the overpressure
183 that might had accumulated before failure. GDF deposits representing MIS 8 (P5, 300-243 ka), which
184 show the best-developed mounded seismic facies on the North Sea TMF (Nygård et al., 2005), overlie
185 the "fill"-fundament and represent MU3. We assume that the deposits representing the MIS 8 deglacial
186 and the MIS 7 interglacial, which cannot be identified in the seismic data, have been eroded by the
187 Tampen Slide. A 10 m thick layer of stratified fine-grained glacimarine sediments is therefore included
188 for this time period, defining MU2 (Fig. 4; Tab. 1). We estimate this layer to have a thickness of 10 m
189 based on deglacial and interglacial sedimentation rates in the study area (Haflidason et al., 1998; Becker
190 et al., 2018). The thickness of the sediments removed by the Tampen Slide (MU1) is estimated based
191 on the intact stratigraphy upwards of the Tampen Slide headwall and extrapolated to simulate pre-failure
192 conditions. We further assume MU1 to be thickest ~20 km downslope of the Tampen Slide headwall,
193 corresponding with the right lateral boundary of the model. Characterized as relatively uniform in its
194 rheological properties, MU1 consists of mainly GDFs deposited during MIS 6 (Tab. 1).

195 Whereas the Storegga Slide developed retrogressively (Gauer et al., 2005), such behavior is not evident
196 from the present seismic data in the Tampen Slide region. As we assume that the Tampen Slide was not
197 initiated by the destabilization of a locally steeper slope, modeling a laterally complete profile is not
198 expected to add significantly to the modeling results. We therefore laterally limit the model domain to
199 40 km, consisting of a 10 km wide continental shelf and 30 km of continental slope. The paleo-slope
200 dip used in the model (0.6°) runs parallel to the basal reflector of the Tampen Slide (Fig. 4).

201 **Sediment properties**

202 The three materials used in the model are characterized by GDFs (MU3), mainly GDFs (MU1) and
203 glacimarine sediments (MU2) (Fig. 4, Tab. 1). All deposits are modelled as non-linear porous

elastoplastic materials, described by the Modified Cam Clay constitutive model. All soil units are inferred to have a Poisson ratio (ν) of 0.3, and a friction angle (φ) of 28°. These values are based on measurements performed on GDFs from a similar geological setting, i.e. the upper-middle continental slope of the Storfjorden TMF (Llopart et al., 2014). The dry density (ρ_{dry}) is 1.8 g/cm^3 for glacimarine deposits and 2.0 g/cm^3 for the GDF-dominated modeling units (Tab. 2) (King et al., 1998).

For the consolidation properties (compressibility (λ) and permeability (k)) we use values measured on samples of glacial debris and glacimarine deposits from the nearby Ormen Lange gas field area on the upper Møre continental slope (Kvalstad et al., 2005a) (Fig. 1, Tab. 2). Even if the composition of glacial sediments is documented to vary in time and space (King et al., 1996), the use of these values can be justified as we expect similar depositional environments and similar sediments to be represented in the neighboring North Sea TMF. The slope of the normal compression line in the Modified Cam Clay model (λ), hereafter referred to as compressibility for simplicity, decreases with decreasing void ratio, averaging at 0.09 for GDFs and 0.29 for glacimarine deposits. The compressibility of mainly glacial debris (MU1) is 0.1 for all void ratios due to lack of consolidation tests for this sediment type. Permeability (k) is a function of porosity (n), and is defined as $\log10(k) = 11.5 \cdot n - 14.6$ for packages consisting of GDFs and mainly GDFs, and $\log10(k) = 7.6 \cdot n - 13.8$ for glacimarine deposits. The void ratio at 1 kPa (e0, void ratio at seafloor) is set to 3.5 (equals a porosity of 0.78) for the glacimarine sediments and 1.2 (equals a porosity of 0.55) for the GDF-dominated modelling units (Tab. 2).

Simulating sediment deposition during MIS 6

We simulate sediment deposition during MIS 6, at the end of which the Tampen Slide occurred, by consecutively "switching on" eight elements rows. Displacement and pore-pressure plane-strain elements are activated and stacked on top of the elements of the model in a sequence of steps. The load is gradually increasing over time within the deposited elements. Pore pressure development and slope stability are analyzed in both the newly deposited as well as the pre-existing sediments during the deposition of the element rows which define MU1.

Back-stripping of the stratigraphy allowed to better estimate the real sediment thicknesses at the time of deposition. Using a calculated decompacted MU1 thickness of ~340 m at the location of the Tampen Slide headwall, each row is ~40 m thick. An average compaction of 30 % caused by rapid glacial sediment loading is comparable to previous studies, in which compaction was estimated to up to 40 % (Hjelstuen et al., 2005).

Meshing, boundary and initial conditions

The mesh used in the modelling consists of 27,000 8-node biquadratic displacement, bilinear pore pressure elements with reduced integration (Fig. 4). The elements have a size of 40x40 m in MU1 and 10x40 m in MU2, while a coarser mesh size was vertically adapted down in the model domain. These differences in element size are reasonable, as the uppermost sediment package is the area of interest and as changes in mechanical properties are less pronounced at larger depths (Hamilton, 1976; Karig and Hou, 1992). The element size also increases towards the lateral boundaries. The model does not allow any displacement at its base, while its lateral boundaries are constrained in the x-direction and free at its top. The lateral-landward and bottom boundaries are impermeable (Fig. 4), whereas fluids are free to flow from the surface, where overpressure is zero. The different model units extend over the entire length of the model domain and are permeable at their upper and lower boundaries (Fig. 4).

For the initial conditions of the model, we assume that the sediments are normally consolidated, with a void ratio defined according to stress conditions and overpressure defined to be zero. This can be justified as (i) a major landslide (Møre Slide; Fig. 2) is assumed to release overpressure and reset the stress regime to overconsolidated conditions with zero excess pore pressure, and (ii) a long interglacial time period (243-191 ka; MIS 7) preceded the time of initiation of our model (Fig. 4), during which large amounts of fluids are expected to have escaped and overpressures to have dissipated as sediments have been deposited at low rates.

3.2 Model runs

Based on the age constrains of sequence P4 and the Tampen Slide (Nygård et al., 2005), we suggest that MU1 represents MIS 6 and that the Tampen Slide was initiated at the end of this MIS (~130 ka). We

initiate our model at the beginning of MIS 6, and then run it in eight steps and a total of 61 kyr, representing the sedimentation history during MIS 6. The added soils are consolidating in the process. Gravitational loads for the individual elements are ramped up during the step, with no load in the beginning and complete load at the end of a step.

Uncertainties in timing and sediment decompaction have a large effect on the sedimentation rates. While the thickness of sequence P4 can be estimated with confidence, there are no age dates available from this 340 m thick sequence. In order to address this uncertainty, we ran models with three different sedimentation scenarios to identify situations in which particularly high pore pressures may be generated.

The first scenario, considered the reference model, uses constant sedimentation rates of 3.3 m/kyr for MIS 6 and geotechnical values measured on samples from nearby locations (Kvalstad et al., 2005a). The goal of the reference model was to evaluate if constant temporal sediment loading has a destabilizing effect. Previous modelling studies have identified compressibility as a key factor for overpressure generation due to sediment deposition (Urlaub et al., 2012; Urlaub et al., 2015). We therefore use a higher compressibility value for the uppermost layer (MU1) than provided by Kvalstad et al. (2005a) in one scenario.

Ice-sheet configurations and sedimentation rates might change during a marine isotope stage (Becker et al., 2018). In the second scenario, the sedimentation rates follow a pattern similar to the last glacial (MIS 2), with an increase in sediment accumulation in the second half of the glacial (Hjelstuen et al., 2004). Such an ice sheet configuration has also been suggested for MIS 8 (Fig. 3) (Nygård et al., 2005). In this scenario, three element rows (equivalent to c. 120 m decompacted sediment) are deposited in the first 30 ka, and five element rows (equivalent to c. 200 m decompacted sediment) in the last 30 ka. This scenario should test if episodically high sedimentation rates may generate a significant amount of overpressure.

Sequence P4 can be separated into three GDF sequences, each having a maximum thickness of 100-200 m (Nygård et al., 2005). These seismostratigraphic observations could indicate rapid on-off switching

of the Norwegian Channel Ice Stream, suggested for other glacials (Nygård et al., 2007; Becker et al., 2018). Thus, in the third scenario, the GDF sequences of MU1 are each defined by two rows of high sedimentation rates. These rows were separated from each other by one row with half the sedimentation rate, and each GDF sequence was then deposited over 12 kyr. This model scenario evaluates the effect of pulses of high sedimentation rates on slope stability.

3.3 Slope stability analysis and earthquake calculation

The overpressure ratio (λ*), defined as the excess pore pressure (p_e) divided by the vertical effective stress (σ'_v) and the excess pore pressure, is a useful measure for the degree of overpressurization of the slope. For example, for a slope gradient of ~1° consisting of homogenous sediment with a friction angle of 30˚, an overpressure ratio of 0.96 is required to induce slope failure without any external force (Urlaub et al., 2015).

$$\lambda^* = \left(\frac{p-p_h}{\sigma_v-p_h}\right) = \frac{p_e}{\sigma'_v+p_e} \quad (1)$$

For the case that overpressure generated by rapid sedimentation is insufficient to initiate slope failure, we couple the 2D Finite Element Modeling with cyclic loading. Earthquakes can contribute to the destabilization of a slope, as the horizontal component of the earthquake acceleration generates shear stresses (Hampton et al., 1996). According to finite slope stability models and following the approach of ten Brink et al. (2009), earthquake-triggered submarine landslides in soft sediments occur when the shear stress on the slip surface exceeds the undrained shear strength of the sediment (e.g. Morgenstern, 1967). This condition is expressed by the Factor of Safety (FoS) as

$$FoS = \frac{\sigma'_v \cdot tan\Phi_{crit}}{\tau+F_{eq}} \quad (2)$$

where σ'_v is the vertical effective stress, Φ_{crit} the critical friction angle, τ the shear stress and F_{eq} the earthquake acceleration shear stress parallel to the slope. In order to initiate slope failure (FoS≤1), we calculate

$$F_{eq} = (\sigma'_v \cdot tan\Phi_{crit}) - \tau \quad (3)$$

In previous studies (ten Brink et al., 2009; Stigall and Dugan, 2010), the critical horizontal earthquake acceleration k_y has been calculated to

$$k_y = \frac{F_{eq}}{\sigma'_v + p_e} = \frac{(\sigma'_v \cdot tan\Phi_{crit}) - \tau}{\sigma'_v + p_e} \quad (4)$$

where p_e is the excess pore pressure.

We follow ten Brink et al. (2009) and link the critical acceleration, k_y, to the spectral acceleration required for triggering slope failure, $k_{PSA(T=0.75)}$, as

$$k_{PSA(T=0.75)} = \frac{k_y}{0.15 \cdot 3.5} \quad (5)$$

This relation is applied by ten Brink et al. (2009) for the slopes offshore Eastern North America which are geologically and tectonically similar to our study area, and assume the relation to be a reasonable choice for our application. We then relate the obtained $k_{PSA(T=0.75)}$-value to earthquake magnitude and distance by considering an empirical ground motion prediction equation (GMPE). As no GMPE has been developed according to modern standards based on Norwegian data, we adopt the recent relation by Pezeshk et al. (2015) which is valid for Eastern North America, where ground motion characteristics are similar to our study area.

4. Results

We assess the effect of different scenarios of temporal sediment loading, compressibility contrasts, and a glacimarine sediment layer on pore pressure generation and slope stability. The results are presented as vertical profiles located 10 km downslope from the shelf break (x = 20 km, Fig. 4). This location represents the Tampen Slide headwall (Fig. 2), and likely the onset of failure assuming that the landslide did not develop retrogressively.

4.1 Reference model

Fig. 5 presents the results of the reference model, characterized by constant sedimentation rates and measured hydro-geomechanical sediment properties (Tab. 3), after the 61 ka long time span of MIS 6. The results show that excess pore pressure (p_e) increases continuously with depth and time (Figs. 5a, 7a-1) to 800 kPa at ~500 m below seafloor (bsf). Below this level, the excess pore pressure increases to 3000 kPa towards the bottom of the model (Fig. 5a). The vertical effective stress (σ'_v) is increasing constantly from 0 kPa at the seafloor to 30000 kPa at the base of the model (Fig. 5b).

The constant sedimentation rates of 3.3 m/kyr during MIS 6 result in maximum overpressure ratios (λ*) of 0.16 at depths of ~200 m bsf, with λ*-values varying from 0.1 to 0.16 within the rapidly-deposited MU1 (Figs. 5c, 7a-2). While λ* rapidly increases during the deposition of the first two rows, its rate of increase is lower during the deposition of the last six rows (Fig. 7a-2). The fluid gradients indicate an eastwards-oriented fluid flow, which is dominated by a vertical component (Fig. 5d). Although sediment depths with maximum overpressure ratios are likely to be affected by the Tampen Slide, less than 16% of the total overburden stress taken up by the excess pore pressure is insufficient to cause slope failure. Thus, constant sedimentation rates in the North Sea TMF during MIS 6 most likely did not generate sufficient excess pore pressure to cause slope failure.

4.1.1 Changes in compressibility

Deterministic sensitivity analyses on models used in previous studies (Urlaub et al., 2015) showed a high sensitivity of overpressure generation to compressibility. Therefore, we also ran the reference model under the assumption that the material characterizing MU1 is more compressible than expected. Therefore, the compressibility of MU1 was increased from 0.1 in the reference model to 0.13 for the compressibility test (Tab. 2, Fig. 6). The results from this model run show that the excess pore pressure rises with a steep gradient from the seafloor to values of 2500 kPa at the base of the highly-compressible layers (Fig. 7b-1), and that the p_e-values are more than doubled compared to the p_e-values in the reference model when using an increased compressibility (Fig. 7a-1). Excess pore pressures increase with a much lower gradient for low-compressible sediment properties in MU1 (Fig. 7a-1). Within the underlying MU3, the excess pore pressures rise with the same gradients for both model runs.

This model run results in overpressure ratios of 0.55 at the top of the glacimarine layer at the profile location (MU2, Figs. 6, 7b-2). The highest overpressure ratios of 0.7 occur at the right–hand-size boundary of the model (Fig. 6b), where the deposited sediment package is thickest. Overpressure ratios decrease both atop and below MU2. Both a normal- and a high-compressible MU1 result in overpressure generation with time, with most of the overpressure generated during the first 15 ka (Figs. 7a-2, 7b-2). However, we note that utilizing a higher compressibility results in more significant overpressure ratio increases between the different time steps (Figs. 7a-2, 7b-2). Thus, the model run shows that an increase

in compressibility from 0.1 to 0.13 has large effects on overpressure generation. An increase of 33 % in compressibility results in an increase of 200 % of overpressure. On the other hand, void ratio values, decreasing through time, are comparable for both the reference and the enhanced compressibility model runs (Figs. 7a-3, 7b-3).

4.1.2 Glacimarine layer

The modelling shows that the highest overpressure ratios occur within the glacimarine layer (Figs. 5-7). Therefore, this unit could represent the level in the model domain which is closest to fail or to act as a slip plane. The overpressure ratio increases with depth, and reaches its maximum values at the top of the glacimarine layer or slightly above (Figs. 7a-2, 7b-2). The glacimarine layer is furthermore characterized by a higher void ratio, which slightly decreases with time (Figs. 7a-3, 7b-3). While excess pore pressures are more or less constant within the glacimarine layer (Fig. 7a-1, 7b-1), the overpressure ratios decrease in this unit (Fig. 7a-2, 7b-2), which probably can be explained by an increase in vertical effective stresses. Similar p_e-gradients are observed for MU1 in the reference model compared to the model scenario from which the glacimarine layer was excluded (Figs. 7a-1, 7c-1). The glacimarine layer results in increased overpressure ratios in MU1 for the compressibility test run (Fig. 7b-1). Removing the glacimarine layer results in lower excess pore pressures and overpressure ratios, and no contrast in the void ratio values (Fig. 7c). The inherited effect of the glacimarine draping sediment layer at the base of the rapidly deposited GDFs is thus an increase in the gradients of both excess pore pressures and overpressure ratios in MU1 as well as a contrast in permeability.

4.2 Variability in sedimentation rates

The first five rows of the model, comprising ~200 m of sediments, were activated after different periods to test the effect of different temporal or staged loading on slope stability. In the reference model (Fig. 8a), these rows were constantly deposited with a rate of 3.3 m/kyr. During this model run, the excess pore pressure and overpressure ratio at the top of the glacimarine layer steadily increase to values of ~450 kPa and 0.13, respectively. While p_e is showing a constant increase in time, λ^* has a stronger rise during the deposition of rows 1 and 3 (Fig. 8a). We also note that the overpressure ratio is highest within the glacimarine layer itself, but that the differences to the neighboring sediments are small.

The model run of an ice-sheet build-up scenario (Fig. 8b), with sedimentation rates of 2.4 m/kyr for the first three rows and increased sedimentation rates of 4.2 m/kyr for the last two rows, results in higher p_e- and λ^*-values at the top of the glacimarine layer compared to the reference model. The excess pore pressure and overpressure ratio increase significantly during the deposition of the first rapidly-loaded row (row 4), and reach a maximum of 0.2 at the depth of the glacimarine layer. The excess pore pressure in MU1 is similar to the excess pore pressure generated in the reference model. The vertical and lateral profiles show that the highest overpressure values of this scenario are not generated within the glacimarine layer, but rather at the interface of the glacimarine layer and the rapidly-deposited GDFs (Fig. 8b).

In the switch on/off scenario (Fig. 8c), excess pore pressures increase during the deposition of the four rapidly-deposited rows (4.2 m/kyr, rows 1-2 and 4-5), whereas no change is observed when deposition is slow (2.1 m/kyr, row 3). Overpressure ratios of 0.2 are generated at the top of the glacimarine layer at the end of both pulses of rapid sedimentation. Episodically high sedimentation rates may generate increases of +300 kPa per row in excess pore pressure and +0.07 per row in overpressure ratio. However, episodically high overpressure dissipation starts once the episode of high load is terminated. During the anticipated switch-off phase of the ice stream, the overpressure ratio is significantly decreasing to values of ~0.1 in the glacimarine layer. Unlike the other two scenarios, the switch on/off scenario shows highest overpressure ratios within MU1 and not in the glacimarine layer where overpressure decreases. At the end of the model run (5 rows or 200 m of sediment), the overpressure ratio is ~0.05 higher compared to the reference model for depths affected by the Tampen Slide.

In summary, these models show that the excess pore pressure increases either continuously or more abruptly in time depending on the sedimentation pattern. However, the overpressure ratio in the glacimarine layer and MU1 generated after the deposition of the five rows do not significantly vary for the different sedimentation patterns. We also observe that episodically high sedimentation rates cannot compensate for the dissipating pore pressure during periods of low sedimentation. Maximum overpressure ratios develop either at the interface between the glacimarine layer and MU1, or within MU1. Rapid sedimentation rates result in maximum overpressured slopes at depths expected to be the

base of the Tampen Slide or above, whereas lower overpressures are generated for constant sedimentation rates. The model shows that the maximum overpressure ratio at the end of row 5 is 0.2, and that the totally generated overpressure is low.

4.3 Slope stability and the effect of seismic shaking

The results obtained from the various models, and particularly the overpressure ratio (λ*) and the Factor of Safety (FoS), were used to analyze slope stability. The FoS, defined by the failure-resisting strength of the sediment divided by failure-inducing stresses (Formula 2), was >1 at any time of deposition, and the slope is therefore considered stable. As sedimentation-related pore pressure generation cannot explain the Tampen Slide, we consider the possibility of having an earthquake as an external trigger mechanism. Highest overpressure ratios (Fig. 7a-2, 7b-2), and shear stress values of up to ~110 kPa are observed within the glacimarine layer of the reference model (Figs. 9a, b), indicating that the slope is closest to failure at this depth not only for the selected profile, but for the entire model. The required additional horizontal loading by earthquakes (F_{eq}) to cause instability is in the order of 1.9 MPa. The critical horizontal earthquake acceleration (k_y) at the location of the Tampen Slide headwall at the depth of the glacimarine layer is calculated to 0.49 g, which corresponds to $k_{PSA(T=0.75)}$ = 0.93 g (Fig. 9c). By applying the empirical ground motion prediction equation of Pezeshk et al. (2015), this level of ground shaking can be generated by an earthquake of magnitude M6.9 or larger in the immediate vicinity of the slide headwall, or by an event with M7.5 or larger at a distance of up to 3.5 km from the Tampen Slide headwall.

5. Discussion

Here, we evaluate the effect of different glacial sedimentation patterns and the 10 m-thick glacimarine sediment layer on overpressure generation and slope stability of the North Sea TMF. Potential trigger mechanisms for the Tampen Slide and future slide activity in the ~1˚-dipping North Sea TMF are discussed based on seismic and overpressure quantification. Finally, we discuss the results from this study in a global perspective.

5.1 Effect of glacial sedimentation patterns on slope stability

442 The modelling shows that excess pore pressures build up due to the deposition of GDFs during MIS 6.
443 The highest excess pore pressures and overpressure ratios are related to increased sediment
444 accumulation in the second half of the model run or during extreme episodic pulses, whereas constant
445 sedimentation rates result in a more stable slope, i.e. with less excess pore pressure generation. However,
446 the magnitude of the resulting overpressure ratios at the end of the glacial stage does not vary
447 significantly between the different models. We explain the lower overpressure ratios generated after
448 time periods with decreased sedimentation rates (Figs. 8b, 8c) by pore pressure dissipation when
449 sedimentation rates were low to medium. The sedimentation rates used for the model are based on
450 stratigraphical constraints (Fig. 2). However, other studies indicate higher sedimentation rates along the
451 Norwegian shelf break (Dimakis et al., 2000; Hjelstuen et al., 2004; Nygård et al., 2007). Previous
452 studies also suggest that shelf-edge glaciations only lasted for short periods (Nygård et al., 2007; Becker
453 et al., 2018). Thus, loading the North Sea TMF over a very short time period with extremely high
454 sediment volumes could generate sufficient overpressure for slope failure. However, in order to fulfill
455 the age constrains of MU1 (61 ka), such periods characterized by extreme loading would have to be
456 compensated by periods characterized by low sedimentation rates, which is rather unlikely during shelf
457 edge glaciations. The model runs indicate that an ice stream needs to be located near the shelf edge for
458 high sedimentation rates to be maintained for most of a glaciation in order to create a slope more
459 vulnerable to fail. Studies from the Gulf of Mexico show that sedimentation rates of 6-9 m/ka resulted
460 in overpressure ratios of 0.7-0.8 (Schneider et al., 2009), indicating that even a doubling of the
461 sedimentation rates at the North Sea TMF would probably not lead to overpressure-driven slope failure.

462 Our models suggest that compressibility has a large effect on overpressure generation (Figs. 6, 7b).
463 Strongly increased overpressure ratios (Fig. 7b-2) indicate that sediments characterized by a higher
464 compressibility could have contributed to slope instability along the gently-dipping seabed of the North
465 Sea TMF. However, compressibility values >0.13 for MU1 would be required to generate sufficient
466 overpressure, which may be within the measuring error. This test showed that small changes in
467 compressibility have a high impact on overpressure generation.

Numerical slope stability analysis of the Santa Barbara basin of the California borderland suggests that pre-conditioning through rapid sedimentation has controlled the emergence of large, slope-parallel landslides on the northern flank of that basin (Stoecklin et al., 2017). However, high sedimentation rates at the North Sea TMF during glacial stages cannot generate sufficient overpressure to cause slope failure on the ~1˚-dipping seabed. Different temporal sedimentation patterns do not significantly affect the amount of overpressure generated at the end of the model runs. The model scenarios assume overpressure to be zero at the beginning of the simulations, which is a rather conservative estimation. The role of ice load on the continental shelf and fluid migration from Miocene ooze layers have not been included as contributing factors to overpressure generation. Glacial unloading related to a melting Norwegian Channel Ice Stream most likely resulted in fluid migration away from the slope and towards the shelf, making the slope more stable. However, as the Norwegian Channel Ice Stream must have been warm-based, and ice overload did not significantly exceed the water column, ice unloading is probably only having a minor effect. Loading and unloading of the slope by ice sheet advances and retreats has been shown to have only minor effects on continental slope stability (Kratzke, 2018), and can thus be neglected.

5.2 Potential of glacimarine deposits acting as a weak layers

Bedding-parallel layers may represent so-called weak layers which play a key role in the development of slope failures (Haflidason et al., 2003; Berg et al., 2005; L'Heureux et al., 2013; Locat et al., 2014). However, slopes have been modelled to be prone to fail along preferential horizons at defined depths without the presence of an intrinsic weak layer (Stoecklin et al., 2017). For the North Sea TMF, observations in the seismic profiles show that sediments mainly consisting of GDFs (MIS 6) have been removed above a package consisting of GDFs (MIS 8) during the Tampen Slide (Fig. 2). We note that no glacimarine sediment package has been resolved in the seismic profile of the study area, but deglaciation packages have been observed for the time periods related to MIS 2 and MIS 6 on the Vøring Plateau (Fig. 1) (Haflidason et al., 2003; Lekens et al., 2005). Therefore, we suggest that such a deglacial and/or interglacial package has also existed in the area affected by the Tampen Slide, but has either been eroded by the megaslide or is too thin to be resolved in the seismic profiles (vertical resolution of c. 10

m, Nygård et al., 2005). The surface parallel to the seafloor, at a depth correlating with the glacimarine sediment deposits, is characterized by highest void ratios, highest overpressure ratios and highest shear stresses (Figs. 7, 9).

The high permeability of the glacimarine layer could have accommodated vertically-oriented fluid flow (Fig. 10a). At the same time the low-permeable overlying package, mainly consisting of GDFs, acted as a barrier for vertical fluid flow. Combining these two effects would explain the highest overpressures at the very top of the glacimarine layer (Fig. 7). Thus, permeability contrasts linked to the glacimarine layer would significantly contribute to the preconditioning of the Tampen Slide. Gas accumulation below GDFs has also been suggested by ocean bottom seismometer investigations in the Storegga Slide area (Mienert et al., 2005b), and support our hypothesis that GDFs are a trap to vertical fluid flow. We suggest fluids to accumulate at the top of the glacimarine layer.

Therefore, we conclude that the glacimarine layer itself or the interface of the glacimarine layer with the overlying GDF-dominated sequence most likely acted as a weak layer for the Tampen Slide (Fig. 10a). Similar failure planes are found in fine-grained depositional units, such as plumite or glacimarine and hemipelagic sediments (Haflidason et al., 2003; Berg et al., 2005), on the mid-Norwegian continental margin, or in laminated glacimarine clays at the upper continental slope off Vesterålen (L'Heureux et al., 2013). Reported excess pore pressures of up to 0.2 within contouritic sediments below GDFs in the Storegga Slide area (Bryn et al., 2003), which also correlate with zones of anomalously low s-wave velocities (Mienert et al., 2005b), support the result of our model simulations. Although the stability at the expected Tampen Slide failure depth is reduced, overpressure-driven slope failure is not suggested.

The effect of sedimentological and geotechnical properties of glacimarine layers beneath rapidly deposited glacial debris has previously been discussed at different locations within the North Atlantic. These layers are reported to have higher water contents and lower shear strengths (Lucchi et al., 2012), and are suggested to develop local overpressure zones (Bryn et al., 2003; Mienert et al., 2005b; Berg et al., 2005; Llopart et al., 2014). Coarser-grained glacial deposits overlain by less-permeable glacial sediments in the Barents Sea have been suggested to be charged by fluids and to act as weak beds (Bellwald and Planke, 2018).

5.3 Quantification of trigger mechanisms of the Tampen Slide

It seems that high sedimentation rates alone did not lead to failure of the Tampen Slide, even if using increased compressibility values for the deposited GDFs in MIS 6. Gas hydrates, indicated by the presence of a bottom simulating reflector, are suggested to have contributed to the triggering of the Storegga Slide (Bünz et al., 2003; Mienert et al., 2005a). However, gas hydrates are rather unlikely to be built within GDFs (Bünz et al., 2003; Mienert et al., 2005a), and no gas hydrate indicators have been observed in conventional seismic profiles of the North Sea TMF. Therefore, gas hydrates are rather unlikely to have acted as an additional fluid source affecting overpressure build-up for the Tampen Slide. However, even if not identified in the seismic profiles, the presence of gas hydrates at the North Sea TMF at the age of the Tampen Slide cannot be excluded.

The Tampen Slide could have been initiated at a locally steeper slope at the lower continental slope (Fig. 2), similarly to which has been proposed for the Storegga Slide (Gauer et al., 2005; Kvalstad et al., 2005b), and then developed retrogressively. However, as the lower slope of the North Sea TMF is beyond the main depocenters of GDFs (Fig. 2), initiation in the steepest region could be problematic for the build-up of sufficient pore pressure. The Miocene ooze layer, suggested to favor increased fluid flow in the lower slopes of the Storegga Slide (Riis et al., 2005), is overlain by a significantly thicker Pleistocene sediment sequence in the North Sea TMF, and has thus not been included in the simulations. As the morphology of the Tampen Slide does not indicate retrogressive slide development (Nygård et al., 2005) and as overpressure does not appear sufficient for slope failure at the position of its headwall, we suggest that an external trigger is the most likely cause for the initiation of the Tampen Slide.

Our model results show that an earthquake of M6.9 or larger at a short distance from the Tampen Slide headwall could have triggered the Tampen Slide (Fig. 10b). At present, there is still a higher seismicity around the Quaternary depocenters than elsewhere along the Norwegian continental margin (Byrkjeland et al., 2000). An earthquake of magnitude M5.4 occurred in the distal part of the North Sea TMF as late as in 1988 (Norwegian National Seismic Network; www.skjelv.no), in an area where no active postglacial faults have been mapped. Faults with the potential for accommodating earthquakes of such magnitudes have not been identified in the North Sea TMF. However, seismic events in response to

549 glacio-isostatic rebound offshore Norway, accommodating earthquakes of M6.5-7 without breaking the
550 surface, are considered to be likely (Bungum et al., 2005). Studies within the Storegga Slide region
551 demonstrated the potential for large postglacial earthquakes to occur and to be able to shake sediment
552 layers to a length and degree, which may lead to slope failure for sediments with a deposition-related
553 low FoS (Solheim et al., 2005; Bungum et al., 2005; Lindholm et al., 2005). Severe seismic loading has
554 also been proposed for slope failures within glacimarine sediments off Vesterålen (L'Heureux et al.,
555 2013). Studies from SE Canadian continental slopes suggest that the build-up of overpressure, linked to
556 deposition of GDFs (Aksu and Hiscott, 1992; Hiscott and Aksu, 1994), allows earthquake-triggered
557 failures along slopes with gradients as low as 1° (Tripsanas et al., 2008; Piper, 2014). An earthquake
558 has also been suggested to be the final trigger for submarine mass movements of slopes controlled by
559 high sedimentation rates in the Santa Barbara Basin (Stoecklin et al., 2017). Thus, we suggest an
560 earthquake at the end of MIS 6, coupled with moderate overpressure from rapid sedimentation, to have
561 acted as the additional driving stress necessary for slope failure for the Tampen Slide (Fig. 10b). This
562 earthquake could either have been triggered by stress changes related to sediment deposited on the North
563 Sea TMF itself or by crustal readjustment after the ice sheet retreat, similar to what has been suggested
564 for large slope failures on the continental slope off SE Canada (Piper et al., 2003). Slope stability is
565 reported to increase with increasing frequencies of earthquakes and decreasing sedimentation rates (ten
566 Brink et al., 2016). Thus, an individual high-magnitude earthquake in this seismically moderate region,
567 characterized by high sedimentation rates during glacial stages, seems to be a possible final trigger
568 mechanism. A high peak spectral acceleration with a short duration will not induce slope failure.
569 However, this point has already been accounted for in the approach we follow (ten Brink et al., 2009).

570 The modelling attempt of this study included only one dimension of earthquake shaking, whereas
571 seismic waves in reality affect the sedimentary sequence in three dimensions (Carlton and Kaynia,
572 2016). The lower earthquake frequencies are closer to the resonance frequency of sediment layers and
573 attenuate more slowly within the sediments. Consequently lower earthquake frequencies have longer
574 durations and a higher potential for fluid mobilization than the higher frequencies. Thus, we suggest that
575 lower earthquake frequencies are more important for slope failure initiation (Kramer, 1996).

Increased submarine landslide activity at glacial-interglacial transitions has previously been documented (Maslin et al., 2004; Owen et al., 2007; Urgeles and Camerlenghi, 2013). We suggest that the earthquake that may have initiated the Tampen Slide took place at the transition into MIS 5, when overpressure ratios and seismic activity are assumed to be highest. This timing probably indicates a large difference between slide initiation at the North Sea TMF and the Storegga Slide, which occurred ~15 kyr after peak glaciation (Haflidason et al., 2005). However, due to sparse chronostratigraphical constrains, we cannot exclude that the Tampen Slide was triggered during the MIS 5 interglacial or later. In that case the Tampen Slide had a similar delay as the Storegga Slide.

5.4 Limitations of the numerical modeling study

The numerical models incorporate uncertainties resulting from the limited resolution of seismic data for reconstruction of the sediment architecture, stratigraphy, as well as a lack of in-situ physical, mechanical, and seismological properties of the prevalent sedimentary units explained below in detail. There are actually no deep-drilling results available from the area, and geotechnical parameters are scarce. Furthermore, high-resolution 3D seismic data were not available either. Thus, the overall results of the numerical modeling conducted in this study should be understood qualitatively and the provided estimates of pore pressure levels and earthquake magnitudes considered as approximations of these values. Nevertheless, the parameters used are based on extensive geohazard assessment investigations for the nearby Ormen Lange gas field development (Kvalstad et al., 2005; and other) in a comparable geological setting. Aiming to test how slope stability changes with increasing overburden stresses, we used a reasonable range of parameters for the numerical simulations.

1) Physical and hydro-geomechanical sediment properties: As no hydro-geomechanical information is available from the North Sea TMF, we used hydro-geomechanical sediment properties measured on samples from the nearby Ormen Lange gas field area (Kvalstad et al., 2005; and others). Even though the composition of glacial sediments are known to vary in time and space (King et al., 1996), the similarity in environmental conditions allow for such a transfer. Due to limits in seismic resolution (max. frequency of c. 10 m; Nygård et al., 2005) and an absence of wells, we summarize the composition of model unit MU1 to be mainly GDFs.

2) Stratigraphy: We simulated sediment deposition during MIS 6, and followed the suggestions that the Tampen Slide occurred at the end of this marine isotope stage (Nygård et al., 2005). However, the chronology of the North Sea TMF and the suggested date of the Tampen Slide, on which we base the sedimentation rates and overpressure build-up, are not well constrained or understood. Improvements in the chronological framework of the North Sea TMF are thus crucial to improve the modeling of sedimentation-related overpressure and triggering of megaslides.

3) Pre-slide stress conditions: Our model further assumed overpressure to be zero at the beginning of the simulations. However, there might be some overpressure at the model initiation, as suggested by lateral fluid migration sourced from Miocene oozes in the explanation of the early Holocene Storegga Slide (Bryn et al., 2005; Riis et al., 2005). However, the pre-slide conditions are impossible to reconstruct with the currently available data.

4) Seismological properties: The model was coupled to seismic shaking, which is based on formulas valid for eastern North America (ten Brink et al., 2009). The input parameters for these formulas are not calibrated against Scandinavia, and might be different for our study area. However, we assume a similar response due to similarities in geological and tectonical settings (Pezeshk et al., 2015). Thus, the earthquake triggering the overpressured slopes of the Tampen Slide could have been of lower magnitude than what we modeled in our study.

5.5 Implications and global relevance

Potential links between climate-controlled sedimentation, slope preconditioning, seismic activity and megasliding are demonstrated by numerical modeling of the Tampen Slide. However, the slopes of the North Sea TMF seem not to have failed in glacial stages with similar sedimentological and seismological conditions to the ones found at the end of MIS 6 (Fig. 3) (Nygård et al., 2005). It is not yet understood why megaslides at the North Sea TMF occurred in some periods characterized by rapid sedimentation, whereas the fan seems not affected by large slope failure in other periods. Megaslides during the last glacial/deglacial cycle have also not been observed along the Barents Sea margin (Hjelstuen et al., 2007). Lateral overpressure migration into the Storegga Slide area (Bryn et al., 2005) or the absence of a deglacial/interglacial sediment package at the base of the GDFs could additionally favor slope stability

630 in this period. The observation that the North Sea TMF did not fail during some shelf edge glaciations
631 generating GDFs supports an earthquake as the ultimate trigger mechanism for the Tampen Slide.

632 This study shows that changing glacial sedimentation patterns are not significant for the build-up of
633 overpressure towards the end of glacial stages, but that the generation of overpressure is more depending
634 on the total sediment overload. Our model runs indicate that overpressure ratios increase at a very low
635 rate during periods characterized by glacial sedimentation, which are supposed to be some magnitudes
636 higher compared to interglacial sedimentation rates (e.g. Lekens et al., 2005; Becker et al., 2018). Low
637 seismicity, low interglacial sedimentation rates, and ongoing overpressure dissipation (Byrkjeland et al.,
638 2000, Haflidason et al., 1998) result in a margin that at present is more stable than shortly after the last
639 glacial retreat. Dissipating overpressures, related to decreased sedimentation rates and fluids being
640 discharged into the modern system, have been reported by Strout and Tjelta (2005) from the Storegga
641 Slide area and by Dugan and Flemings (2002) for the New Jersey margin. However, dissipating
642 overpressures in the region of the North Sea TMF indicate that overpressures might still be present in
643 the shallow sub-surface of the study area (Fig. 10b).

644 The effect of a glacimarine layer at the base of a package dominated by GDFs is modeled in this study,
645 and could be applied to different TMF systems and glacially-affected margins all over the globe. The
646 deposition of such thin layers seems to be fundamental for the evaluation of major slope failure in
647 different glacial-interglacial cycles. However, there are still numerous uncertainties about weak layers.
648 Probably required for megaslides, our knowledge about the thickness and geotechnical properties of
649 these layers is limited. High-resolution 3D seismic data and deep boreholes for in-situ logging and
650 sampling for geological and geotechnical data will also contribute to a better characterization of weak
651 layers. High-resolution seismic data are also expected to resolve geological expressions on a meter-scale
652 and provide information related to overpressure and fan morphologies relevant for fluid migration.

653 Packages of GDFs overlying the glacimarine layer are suggested to act as seals for vertical fluid flow.
654 Glacial sediments trapping fluids below have been observed in other previously glaciated environments
655 (Dumke et al., 2014; Bellwald and Planke, 2018).

Similar to what has been assumed for the Storegga Slide region (Kvalstad et al., 2005a), we suggest that a strong earthquake is the only realistic trigger for a new submarine megaslide at the North Sea TMF. This earthquake has probably to be of higher magnitude than what we modeled for the overpressure-preconditioned slope at the time of the Tampen Slide. It is, therefore, fair to state that today's hazard of megasliding and tsunami originating from the North Sea TMF is considerably small, and that it will probably take another interglacial-glacial cycle and/or a strong earthquake to form a situation that would lead to another major landslide on the North Sea TMF.

6. Conclusions

In this study we model overpressure and slope stability along the gently-dipping (<1°) North Sea TMF, with the focus to capture stress conditions leading to the development of the Tampen Slide. The influence of sedimentation rate and sediment compressibility on strength reduction on glacial margin submarine slopes has been quantified within the model simulations. However, the results of model simulations should be understood in a qualitative way.

Slope stability has been modeled for a scenario with shelf edge glaciations, ice sheet build-up and ice sheet oscillations during MIS 6, at the end of which the Tampen Slide occurred. As these different configurations result in significant differences in sediment delivery to the study site, we simulate slope stability with different sedimentation patterns, which according to our model result in similar levels of excess pore pressure. Highest overpressure ratios of 0.2 are generated at the interface of an inferred glacimarine layer, when utilizing sedimentation rates of ~4.2 m/kyr for the deposition of GDFs during ice-stream maxima. Constant sediment accumulation of 3.3 m/kyr results in an overpressure ratio of 0.16. Tests with higher compressibilities of GDFs (0.13 instead of 0.10), on the other hand, result in maximum overpressure ratios of 0.55 at the top of an assumed glacimarine layer, which is located below a package consisting of GDFs. As the absence of the glacimarine layer decreases the overpressure ratio, the inherited permeability contrast of this layer is suggested to be fundamental for slope failures to be initiated at the North Sea TMF. The glacimarine layer is suggested to accommodate vertical fluid flow, which is initiated by the rapid deposition of GDFs, which are further acting as a barrier for vertical fluid

683 flow. The modeling suggests that excess pore pressure alone is not sufficient to destabilize the ~300 m-
684 thick sequence of mainly GDFs, which have been removed by the Tampen Slide. Thus, an earthquake
685 of magnitude M6.9 or larger, close to the Tampen Slide headwall, is suggested to have caused slope
686 failure at the time of the Tampen Slide. Even if such a magnitude event has never been historically
687 documented in Scandinavia, seismicity related to stresses induced by post-glacial isostacy at the time of
688 the Tampen Slide is expected to have been significantly higher than at present, allowing for frequent
689 occurrence of such events.

690 This case study has several implications for TMFs and glaciated margins all over the globe. The model
691 runs showed that overpressure mainly depends on the thickness of sediment overburden, and not on the
692 temporal pattern of glacial deposition. Small changes in the model input parameters, such as
693 compressibility values of glacial sediments, have a big effect on overpressure generation. Geological
694 weak layers seem to be required for megaslides along gently-dipping glaciated margins. However,
695 overpressure alone is not capable of causing failure on these slopes. The modeling suggests that
696 increased seismic activity is the final trigger mechanism for the Tampen Slide.

Notation

λ	logarithmic bulk modulus, "compressibility", dimensionless
λ^*	overpressure ratio, dimensionless
ν	Poisson ratio, dimensionless
Φ_{crit}	effective angle of friction, °, critical angle of friction, shearing resistance
ρ_{dry}	dry density, kg/m^3
σ_v	vertical stress, kPa
σ'_v	vertical effective stress, kPa
τ	shear stress, kPa
φ	friction angle, °
e	void ratio, dimensionless
k	permeability, m/s
n	porosity, dimensionless
p	pore pressure, kPa
p_e	excess pore pressure, kPa
p_h	hydrostatic pore pressure
FoS	Factor of safety
F_{eq}	Earthquake acceleration shear stress parallel to the slope
k_{PSA}	Peak spectral acceleration
k_y	Critical horizontal earthquake acceleration

Formula

1) Void ratio $e = \frac{n}{1-n}$

2) Compressibility $\lambda = -\left(\frac{1}{V}\right) \cdot \left(\frac{dV}{dp}\right)$ and $\lambda = \frac{ln(p)}{n}$

3) Overpressure ratio $\lambda^* = \left(\frac{p-p_h}{\sigma_v-p_h}\right) = \frac{p_e}{\sigma'_v+p_e}$

4) Factor of safety $FoS = \frac{\sigma'_v \cdot tan\phi_{crit}}{\tau+F_{eq}}$

5) Required earthquake acceleration shear stress parallel to the slope $F_{eq} = (\sigma'_v \cdot tan\Phi_{crit}) - \tau$

6) Critical horizontal earthquake acceleration $k_y = \frac{F_{eq}}{\sigma'_v+p_e}$

7) Peak spectral acceleration $k_{PSA} = \frac{k_y}{0.15\ x\ 3.5}$

Acknowledgements: We thank Flavio Anselmetti and David J.W. Piper for thorough discussions and constructive feedback. The research leading to these results has received funding from the People Programme (Marie Curie Actions) of the European Union's Seventh Framework Programme FP7/2007-2013/ under REA grant agreement n° 317217. The research forms part of the GLANAM (GLAciated North Atlantic Margins) Initial Training Network. We are grateful to two anonymous reviewers and Editor Henning Bauch for constructive remarks that helped improve the quality of the manuscript.

References:

Aksu, A.E., Hiscott, R.N., 1992. Shingled Upper Quaternary debris flow lenses on the NE Newfoundland slope. Sedimentology 39, 193-206.

Batchelor, C.L., Ottesen, D., Dowdeswell, J.A., 2017. Quaternary evolution of the northern North Sea margin through glacigenic debris-flow and contourite deposition. Journal of Quaternary Science 32, 416-426.

Becker, L.W.M., Sejrup, H.P., Hjelstuen, B.O., Haflidason, H., Dokken, T.M., 2018. Ocean-ice sheet interaction along the SE Nordic Seas margin from 35 to15 ka BP. Marine Geology 402, 99-117.

Bellwald, B., Planke, S., 2018. Shear margin moraine, mass transport deposits, and soft beds revealed by high-resolution P-Cable 3D seismic data in the Hoop Area, Barents Sea. Special publication, Geological Society of London.

Berg, K., Solheim, A., Bryn, P., 2005. The Pleistocene to recent geological development of the Ormen Lange area. Marine and Petroleum Geology 22, 45-56.

Bryn, P., Solheim, A., Berg, K., Lien, R., Forsberg, C.F., Haflidason, H., Ottesen, D., Rise, L., 2003. The Storegga Slide complex: repeated large scale sliding in response to climatic cyclicity. In: Locat, J. and Mienert, J. (Eds.), Submarine Mass Movements and Their Consequences, Advances in Natural and Technological Hazard Research, 215-222.

Bryn, P., Berg, K., Forsberg, C.F., Solheim, A., Kvalstad, T.J., 2005. Explaining the Storegga Slide. Marine and Petroleum Geology 22, 11-19.

Bungum, H., Lindholm, C., Faleide, J.I., 2005. Postglacial seismicity offshore mid-Norway with emphasis on spatio-temporal-magnitudal variations. Marine and Petroleum Geology 22, 137-148.

Bünz, S., Mienert, J., Berndt, C., 2003. Geological controls on the Storegga gas-hydrate system of the mid-Norwegian continental margin. Earth and Planetary Science Letters 209, 291-307.

Byrkjeland, U., Bungum, H., Eldholm, O., 2000. Seismotectonics of the Norwegian continental margin. Journal of Geophysical Research 105, 6221-6236.

Canals, M., Lastras, G., Urgeles, R., Casamor, J.L., Mienert, J., Cattaneo, A., De Batist, M., Haflidason, H., Imbo, Y., Laberg, J.S., Locat, J., Long, D., Longva, O., Masson, D.G., Sultan, N., Trincardi, F., Bryn, P., 2004. Slope failure dynamics and impacts from seafloor and shallow sub-seafloor geophysical data: case studies from the COSTA project. Marine Geology 213, 9-72.

Carlton, B.D., Kaynia, A.M., 2016. Comparison of the Seismic Response of Offshore Slopes Using 1, 2 or 3 Ground Motion Components. Offshore Technology Conference OTC-26961-MS, 1-12.

Dimakis, P., Elverhøi, A., Høeg, K., Solheim, A., Harbitz, C., Laberg, J.S., Vorren, T.O., Marr, J., 2000. Submarine slope stability on high-latitude glaciated Svalbard-Barents Sea margin. Marine Geology 162, 303-316.

Dugan, B., Sheahan, T.C., 2012. Offshore sediment overpressures of passive margins: Mechanisms, measurement, and models. Reviews of Geophysics 50, RG3001.

Dumke, I., Berndt, C., Crutchley, G.J., Krause, S., Liebetrau, V., Gay, A., Couillard, M., 2014. Seal bypass at the Giant Gjallar Vent (Norwegian Sea): Indications for a new phase of fluid venting at a 56-Ma-old fluid migration system. Marine Geology 351, 38-52.

Elverhøi, A., Norem, H., Andersen, E.S., Dowdeswell, J.A., Fossen, I., Haflidason, H., Kenyon, N.H., Laberg, J.S., King, E.L., Sejrup, H.P., Solheim, A., Vorren, T., 1997. On the origin and flow behavior of submarine slides on deep-sea fans along the Norwegian-Barents Sea continental margin. Geo-Marine Letters 17. 119-125.

779 Fischer, D., Mogollón, J.M., Strasser, M., Pape, T., Bohrmann, G., Fekete, N., Spiess, V., Kasten, S.,
780 2013. Subduction zone earthquakes as potential trigger of submarine hydrocarbon seepage. Nature
781 Geoscience 6, 647-651.

782 Flemings, P.B., Long, H., Dugan, B., Germaine, J., John, C.M., Behrmann, J.H., Sawyer, D., IODP
783 Expedition 308 Scientists, 2008. Pore pressure penetrometers document high overpressure near the
784 seafloor where multiple submarine landslides have occurred on the continental slope, offshore
785 Louisiana, Gulf of Mexico. Earth and Planetary Science Letters 269, 309-325.

786 Gales, J., Hillenbrand, C.D., Larter, R., Laberg, J.S., Melles, M., Benetti, S., Passchier, S., 2018.
787 Processes influencing differences in Arctic and Antarctic Trough Mouth Fan sedimentology.
788 Geological Society of London, Special Publications.

789 Gauer, P., Kvalstad, T.J., Forsberg, C.F., Bryn, P., Berg, K., 2005. The last phase of the Storegga Slide:
790 simulation of retrogressive slide dynamics and comparison with slide-scar morphology. Marine and
791 Petroleum Geology 22, 171-178.

792 Haflidason, H., King, E.L., Sejrup, H.P., 1998. Late Weichselian and Holocene sediment fluxes of the
793 northern North Sea Margin. Marine Geology 152, 189-215.

794 Haflidason, H., Sejrup, H.P, Berstad, I.M., Nygård, A., Richter, T., Bryn, P., Lien, R., Berg, K., 2003.
795 A Weak Layer Feature on the Northern Storegga Slide Escarpment, in: Mienert, J. et al. (Eds.),
796 European Margin Sediment Dynamics, Springer-Verlag Berlin Heidelberg, 55-62.

797 Haflidason, H., Lien, R., Sejrup, H.P., Forsberg, C.F., Bryn, P., 2005. The dating and morphology of
798 the Storegga Slide. Marine and Petroleum Geology 22, 123-136.

799 Hamilton, E.L., 1976. Variations of density and porosity with depth in deep-sea sediments. Journal of
800 Sedimentary Petrology 46, 280-300.

801 Hampton, M.A., Lee, H.J., Locat, J., 1996. Submarine landslides. Reviews of Geophysics 34, 33-59.

802 Hiscott, R.N., Aksu, A.E., 1996. Quaternary Sedimentary Processes and Budgets in Orphan Basin,
803 Southwestern Labrador Sea. Quaternary Research 45, 160-175.

Hjelstuen, B.O., Sejrup, H.P., Haflidason, H., Nygård, A., Berstad, I.M., Knorr, G., 2004. Late Quaternary seismic stratigraphy and geological development of the south Vøring margin, Norwegian Sea. Quaternary Science Reviews 23, 1847-1865.

Hjelstuen, B.O., Sejrup, H.P., Haflidason, H., Nygård, A., Ceramicola, S., Bryn, P., 2005. Late Cenozoic glacial history and evolution of the Storegga Slide area and adjacent slide flank regions, Norwegian continental margin. Marine and Petroleum Geology 22, 57-70.

Hjelstuen, B.O., Eldholm, O., Faleide, J.I., 2007. Recurrent Pleistocene mega-failures on the SW Barents Sea margin. Earth and Planetary Science Letters 258, 605-618.

Hjelstuen, B.O., Nygård, A., Sejrup, H.P., Haflidason, H., 2012. Quaternary denudation of southern Fennoscandia – evidence from the marine realm. Boreas 41, 379-390.

Hjelstuen, B.O., Grinde, S., 2016. 3D Seismic Investigations of Pleistocene Mass Transport Deposits and Glacigenic Debris Flows on the North Sea Fan, NE Atlantic Margin, in: Lamarche, G. et al. (Eds.), Submarine Mass Movements and Their Consequences, Advances in Natural and Technological Hazard research, 265-272.

Hooke, R.L., Elverhøi, A., 1996. Sediment flux from a fjord during glacial periods, Isfjorden, Spitsbergen. Global and Planetary Change 12, 237-249.

Hühnerbach, V., Masson, D., partners of the COSTA-Project, 2004. Landslides in the North Atlantic and its adjacent seas: an analysis of their morphology, setting and behaviour. Marine Geology 213, 343-362.

Jibson, R.W., 2011. Methods for assessing the stability of slopes during earthquakes – A retrospective. Engineering Geology 122, 43-50.

Karig, D.E., Hou, G., 1992. High-stress Consolidation Experiments and Their Geologic Implications. Journal of Geophysical Research 97, 289-300.

King, E.L., Sejrup, H.P., Haflidason, H., Elverhøi, A., Aarseth, I., 1996. Quaternary seismic stratigraphy of the North Sea Fan: glacially-fed gravity flow aprons, hemipelagic sediments, and large submarine slides. Marine Geology 130, 293-315.

King, E.L., Haflidason, H., Sejrup, H.P., Løvlie, R., 1998. Glacigenic debris flows on the North Sea Trough Mouth Fan during ice stream maxima. Marine Geology 152, 217-246.

Kramer, S.L., 1996. Geotechnical earthquake engineering. Prentice Hall, Upper Saddle River, N.J.

Kratzke, I.C.J., 2018. Testing the effect of ice sheet dynamics on submarine slope stability by means of finite element modeling. Master Thesis, Kiel University, 59 pp.

Kvalstad, T.J., Nadim, F., Kaynia, A.M., Mokkelbost, K.H., Bryn, P., 2005a. Soil conditions and slope stability in the Ormen Lange area. Marine and Petroleum Geology 22, 299-310.

Kvalstad, T.J., Andresen, L., Forsberg, C.F., Berg, K., Bryn, P., Wangen, M., 2005b. The Storegga Slide: evaluation of triggering sources and slide mechanics. Marine and Petroleum Geology 22, 245-256.

Laberg, J.S., Vorren, T.O., 1996. The Middle and Late Pleistocene evolution of the Bear Island Trough Mouth Fan. Global Planetary Change 12, 309-330.

Lee, H.J., Locat, J., Dartnell, P., Minasian, D, Wong, F., 2000. A GIS-based regional analysis of the potential for shallow-seated submarine slope failure. Paper presented at 8th International Symposium on Landslides, Br. Geotech Soc., Cardiff, Wales, June 2000, 26-30.

Lee, 2009. Timing and occurrence of large submarine landslides on the Atlantic Ocean margin. Marine Geology 264, 53-64.

Lekens, W.A.H., Sejrup, H.P., Haflidason, H., Petersen, G.Ø., Hjelstuen, B., Knorr, G., 2005. Laminated sediments preceding Heinrich event 1 in the Northern North Sea and Southern Norwegian Sea: Origin, processes and regional linkage. Marine Geology 216, 27-50.

Leynaud, D., Mienert, J., Vanneste, M., 2009. Submarine mass movements on glaciated and non-glaciated European continental margins: A review of triggering mechanisms and preconditions to failure. Marine and Petroleum Geology 26, 618-632.

L'Heureux, J.S., Vanneste, M., Rise, L., Brendryen, J., Forsberg, C.F., Nadim, F., Longva, O., Chand, S., Kvalstad, T.J., Haflidason, H., 2013. Stability, mobility and failure mechanism for landslides at the upper continental slope off Vesterålen, Norway. Marine Geology 346, 192-207.

Lindholm, C., Roth, M., Bungum, H., Faleide, J.I., 2005. Probabilistic and deterministic seismic hazard results and influence of the sedimentary Møre Basin, NE Atlantic. Marine and Petroleum Geology 22, 149-160.

Llopart, J., Urgeles, R., Camerlenghi, A., Lucchi, R.G., De Mol, B., Rebesco, M., Pedrosa, M.T., 2014. Slope Instability of Glaciated Continental Margins: Constraints from Permeability-Compressibility Tests and Hydrogeological Modeling off Storfjorden, NW Barents Sea. in: Krastel, S. et al., (Eds.), Submarine Mass Movements and Their Consequences, Advances in Natural and Technological Hazard Research 37, 95-104.

Locat, J., Leroueil, S., Locat, A., Lee, H., 2014. Weak Layers: Their Definition and Classification from a Geotechnical Perspective. In: Krastel, S. et al., (Eds.) Submarine Mass Movements and Their Consequences, Advances in Natural and Technological Hazard Research 37, 3-12.

Lucchi, R.G., Pedrosa, M.T., Camerlenghi, A., 2012. Recent submarine landslides on the continental slope of Storfjorden and Kveitehola Trough – Mouth Fans (NW Barents Sea). In: Yamada, Y. et al., (Eds.), Submarine Mass Movements and Their Consequences, Advances in Natural and Technological Hazard Research 31, 735-745.

Maslin, M., Owen, M., Day, S., Long, D., 2004. Linking continental-slope failures and climate change: Testing the clathrate gun hypothesis. Geology 32, 53-56.

873 Masson, Harbitz, C.B., Wynn, R.B., Pedersen, G., Løvholt, F., 2006. Submarine landslides: processes,
874 triggers and hazard prediction. Philosophical Transactions. Series A, Mathematical, Physical and
875 Engineering Sciences 364, 2009-2039.

876 Masson, D.G., Wynn, R.B., Talling, P.J., 2010. Large landslides on passive continental margins:
877 Processes, hypotheses and outstanding questions. In: Mosher, D.C. et al., (Eds.), Submarine Mass
878 Movements and Their Consequences, Advances in Natural and Technological Hazard Research 28,
879 153-165.

880 McAdoo, B.G., Pratson, L.F., Orange, D.L., 2000. Submarine landslide geomorphology, US continental
881 slope. Marine Geology 169, 103-136.

882 Mienert, J., Vanneste, M., Bünz, S., Andreassen, K., Haflidason, H., Sejrup, H.P., 2005a. Ocean
883 warming and gas hydrate stability on the mid-Norwegian margin at the Storegga Slide. Marine and
884 Petroleum Geology 22, 233-244.

885 Mienert, J., Bünz, S., Guidard, S., Vanneste, M., Berndt, C., 2005b. Ocean bottom seismometer
886 investigations in the Ormen Lange area offshore mid-Norway provide evidence for shallow gas
887 layers in subsurface sediments. Marine and Petroleum Geology 22, 287-297.

888 Morgenstern, N.R., 1967. Submarine slumping and the initiation of turbidity currents. In: Richards, A.F.
889 (Ed.), Marine Geotechnique. University of Illinois Press, Urbana, IL, 189-210.

890 Nygård, A., Sejrup, H.P., Haflidason, H., King, E.L., 2002. Geometry and genesis of glacigenic debris
891 flows on the North Sea Fan: TOBI imagery and deep-tow boomer evidence. Marine Geology 188,
892 15-33.

893 Nygård, A., Sejrup, H.P., Haflidason, H., Bryn, P., 2005. The glacial North Sea Fan, southern Norwegian
894 Margin: architecture and evolution from the upper continental slope to the deep-sea basin. Marine
895 and Petroleum Geology 22, 71-84.

Nygård, A., Sejrup, H.P., Haflidason, H., Lekens, W.A.H., Clark, C.D., Bigg, G.R., 2007. Extreme sediment and ice discharge from marine-based ice streams: New evidence from the North Sea. Geology 35, 395-398.

Owen, M., Day, S., Maslin, M., 2007. Late Pleistocene submarine mass movements: occurrence and causes. Quaternary Science Reviews 7-8, 958-978.

Pezeshk, S., Zandieh, A., Campbell, K.W. and Tavakoli, B., 2015. Ground-Motion Prediction Equations for CENA Using the Hybrid Empirical Method in Conjunction with NGA-West2 Empirical Ground-Motion Models, in Pacific Earthquake Engineering Research Center (PEER), NGA-East: Median Ground-Motion Models for the Central and Eastern North America Region, PEER Report No. 2015/04, 351 pp.

Piper, D.J.W., Mosher, D.C., Gauley, B.J., Jenner, K., Campell, D.C., 2003. The chronology and recurrence of submarine mass movements on the continental slope off southeastern Canada. In: Locat, J. and Mienert, J. (Eds.), Submarine Mass Movements and Their Consequences, Advances in Natural and Technological Hazard Research, 299-306.

Piper, D.J.W., 2014. Process, time and architecture: lessons from slope contourites and their failures in the path of the Labrador Current. 2nd Deep-Water Circulation Congress, Ghent, Belgium, September 2014, 3-4.

Pope, E.L., Talling, P.J., Carter, L., 2017. Which earthquakes trigger damaging submarine mass movements: Insights from a global record of submarine cable breaks? Marine Geology 384, 131-146.

Pope, E.L., Talling, P.J., O'Cofaigh, C., 2018. The relationship between ice sheets and submarine mass movements in the Nordic Seas during the Quaternary. Earth-Science Reviews 178, 208-256.

Rebesco, M., Laberg, J.S., Pedrosa, M.T., Camerlenghi, A., Lucchi, R.G., Zgur, F., Wardell, N., 2013. Onset and growth of Trough-Mouth Fans on the North-Western Barents Sea margin – implications for the evolution of the Barents Sea/Svalbard Ice Sheet. Quaternary Science Reviews 92, 227-234.

921 Riis, F., Berg, K., Cartwright, J., Eidvin, T., Hansch, K., 2005. Formation of large, crater-like evacuation
922 structures in ooze sediments in the Norwegian Sea. Possible implications for the development of the
923 Storegga Slide. Marine and Petroleum Geology 22, 257-274.

924 Schneider, J., Flemings, P.B., Dugan, B., Long, H., Germaine, J.T., Overpressure and consolidation near
925 the seafloor of Brazos-Trinity Basin IV, northwest deepwater Gulf of Mexico. Journal of
926 Geophysical Research 114, B05102.

927 Sejrup, H.P., King, E.L., Aarseth, I., Haflidason, H., Elverhøi, A., 1996. Quaternary erosion and
928 depositional processes: western Norwegian fjords, Norwegian Channel and North Sea Fan.
929 Geological Society Special Publication 117, 187-202.

930 Sejrup, H.P., Larsen, E., Haflidason, H., Berstad, I.M., Hjelstuen, B.O., Jonsdottir, H., King, E.L.,
931 Landvik, J., Longva, O., Nygård, A., Ottesen, D., Raunholm, S., Rise, L., Stalsberg, K., 2003.
932 Configuration, history and impact of the Norwegian Channel Ice Stream. Boreas 32, 18-36.

933 Sejrup, H.P., Haflidason, H., Hjelstuen, B.O., Nygård, A., Bryn, P., Lien, R., 2004. Pleistocene
934 development of the SE Nordic Seas margin. Marine Geology 213, 169-200.

935 Sejrup, H.P., Hjelstuen, B.O., Dahlgren, K.I.T., Haflidason, H., Kuijpers, A., Nygård, A., Praeg, D.,
936 Stoker, M.S., Vorren, T.O., 2005. Pleistocene glacial history of the NW European continental
937 margin. Marine and Petroleum Geology 22, 1111-1129.

938 Skene, K.I., Piper, D.J.W., Aksu, A.E., Syvitski, J.P.M., 1998. Evaluation of the global oxygen isotope
939 curve as a proxy for Quaternary sea level by modeling of delta progradation. Journal of Sedimentary
940 Research 68, 1077-1092.

941 Solheim, A., Bryn, P., Sejrup, H.P., Mienert, J., Berg, K., 2005. Ormen Lange – an integrated study for
942 the safe development of a deep-water gas field within the Storegga Slide Complex, NE Atlantic
943 continental margin; executive summary. Marine and Petroleum Geology 22, 1-10.

944 Stigall, J., Dugan, B., 2010. Overpressure and earthquake initiated slope failure in the Ursa region,
945 northern Gulf of Mexico. Journal of Geophysical Research 115, 167-178.

946 Stoecklin, A., Friedli, B., Puzrin, A.M., 2017. Sedimentation as a control for large submarine landslides
947 – mechanical modelling and analysis of the Santa Barbara basin. Journal of Geophysical Research
948 122 (11), 8645-8663.

949 Strout, J.M., Tjelta, T.I., 2005. In situ pore pressures: what is their significance and how can they be
950 reliably measured? Marine and Petroleum Geology 22, 275-286.

951 Swarbrick, R.E., Osborne, M.J., 1998. Mechanisms that Generate Abnormal Pressures: an Overview.
952 In: Law, B.E. et al. (Eds.), AAPG Memoir 70, 13-34.

953 ten Brink, U.S., Lee, H.J., Geist, E.L., Twichell, D., 2009. Assessment of tsunami hazard to the U.S.
954 East Coast using relationships between submarine landslides and earthquakes. Marine Geology 264,
955 65-73.

956 ten Brink, U.S., Andrews, B.D., Miller, N.C., 2016. Seismicity and sedimentation rate effects on
957 submarine slope stability. Geology 44, 563-566.

958 Tishchenko, P., Hensen, C., Wallmann, K., Wong, C.S., 2005. Calculation of the stability and solubility
959 of methane hydrate in seawater. Chemical Geology 219, 37-52.

960 Tripsanas, E.K., Piper, D.J.W., Campell, C., 2008. Evolution and depositional structure of earthquake-
961 induced mass movements and gravity flows: Southwest Orphan Basin, Labrador Sea. Marine and
962 Petroleum Geology 25, 645-662.

963 Twichell, D.C., Chaytor, J.D., ten Brink, U.S., Buczkowski, B., 2009. Morphology of late Quaternary
964 submarine landslides along the U.S. Atlantic continental margin. Marine Geology 264, 4-15.

965 Urgeles, R., Camerlenghi, A., 2013. Submarine landslides of the Mediterranean Sea: Trigger
966 mechanisms, dynamics, and frequency-magnitude distribution. Journal of Geophysical Research
967 118, 2600-2618.

968 Urlaub, M., Zervos, A., Talling, P.J., Masson, D.G., Clayton, C.I., 2012. How do 2° slopes fail in areas
969 of slow sedimentation? A sensitivity study on the influence of accumulation rate and permeability

on submarine slope stability. In: Yamada, Y. et al., (Eds.) Submarine Mass Movements and Their Consequences, Advances in Natural and Technological Hazard Research 31, 277-287.

Urlaub, M., Talling, P.J., Zervos, A., Masson, D., 2015. What causes large submarine landslides on low gradient (<2°) continental slopes with slow (~0.15 m/kyr) sediment accumulation? Journal of Geophysical Research: Solid Earth 120, 6722-6739.

Urlaub, M., Geersen, J., Krastel, S., Schwenk, T., 2018. Diatom ooze: Crucial for the generation of submarine mega-slides? Geology 46, 331-334.

Vanneste, M., Sultan, N., Garziglia, S., Forsberg, C.F., L'Heureux, J.S., 2014. Seafloor instabilities and sediment deformation processes: The need for integrated, multi-disciplinary investigations. Marine Geology 352, 183-214.

Vanneste, M., L'Heureux, J.S., Baeten, N., Brendryen, J., Vardy, M.E., Steiner, A., Forsberg, C.F., Kvalstad, T.J., Laberg, J.S., Chand, S., Longva, O., Rise, L., Haflidason, H., Hjelstuen, B.O., Forwick, M., Morgan, E., Lecomte, I., Kopf, A., Vorren, T.O., Reichel, T., 2012. Shallow Landslides and Their Dynamics in Coastal and Deepwater Environments, Norway. In: Yamada, Y. et al., (Eds.), Submarine Mass Movements and Their Consequences, Advances in Natural and Technological Hazard Research 31, 29-41.

Vorren, T.O., Laberg, J.S., 1997. Trough mouth fans – paleoclimate and ice-sheet monitors. Quaternary Science Reviews 16, 865-881.

Vorren, T.O., Laberg, J.S., Blaume, F., Dowdeswell, J.A., Kenyon, N.A., Mienert, J., Rumohr, J., Werner, F., 1998. The Norwegian-Greenland sea continental margins: morphology and late Quaternary sedimentary processes and environment. Quaternary Science Reviews 17, 273-302.

www.skjelv.no, Norwegian National Seismic Network, Bergen, Norway, 15.08.2016

www.vectorworldmap.com, Vector World Map, Graphics Factory CC, Pretoria, South Africa, 15.08.2016.

995 **Figures:**

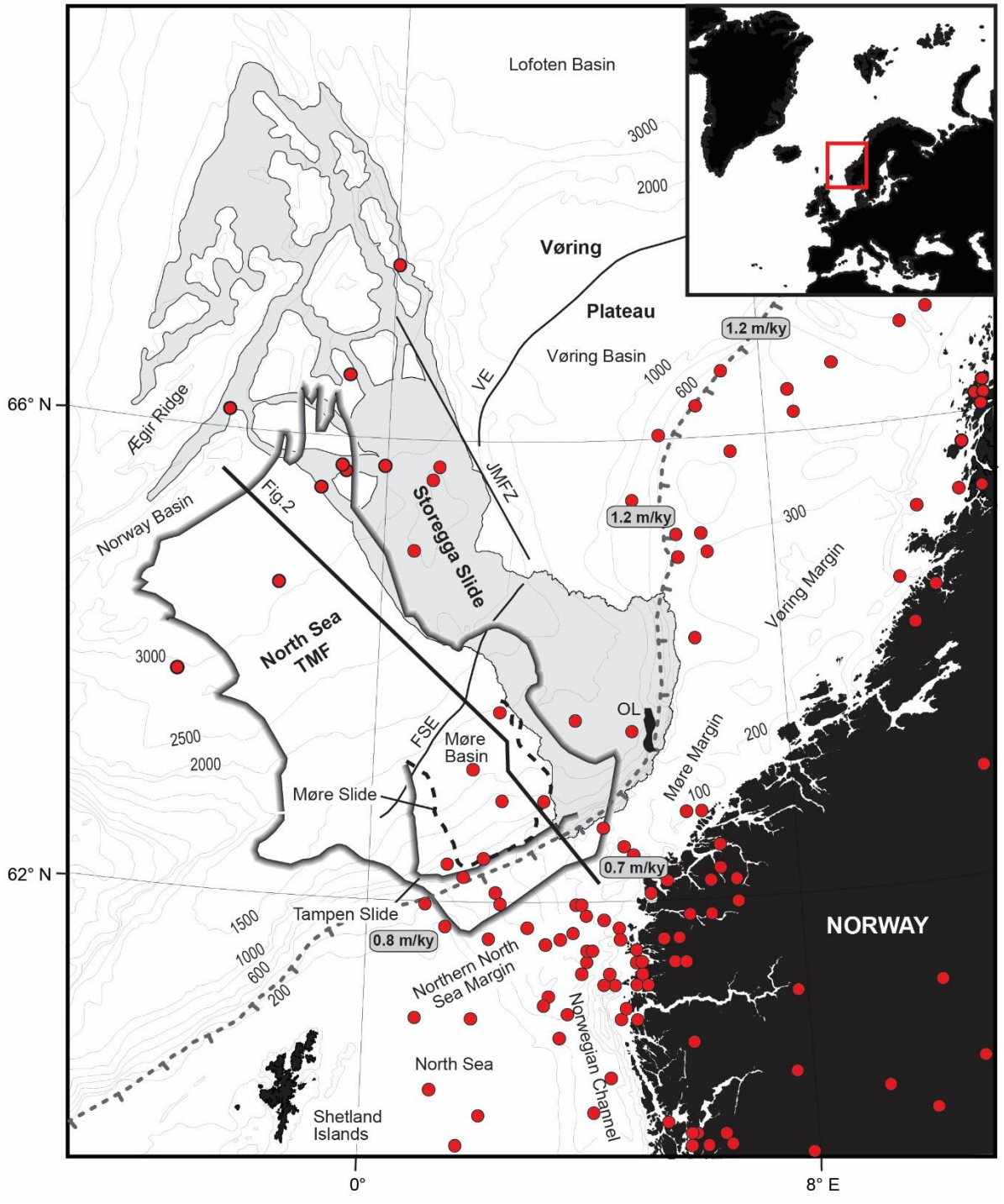

996

997 **Fig. 1.** The Norwegian continental margin with outline of identified submarine slides and the North Sea
998 trough mouth fan (TMF). Stippled gray line indicates maximum ice sheet extent during the Last Glacial
999 Maximum (Sejrup et al., 2016) and numbers in gray boxes indicate subsidence rates (Sejrup et al., 2004).
1000 Earthquakes with magnitudes M>4 since 1970 are shown (Norwegian National Seismic Network,
1001 www.skjelv.no). FSE: Faroe-Shetland Escarpment, JMFZ: Jan Mayen Fracture Zone, OL: Ormen Lange
1002 gas field, VE: Vøring Escarpment. World map from www.vectorworldmap.com.

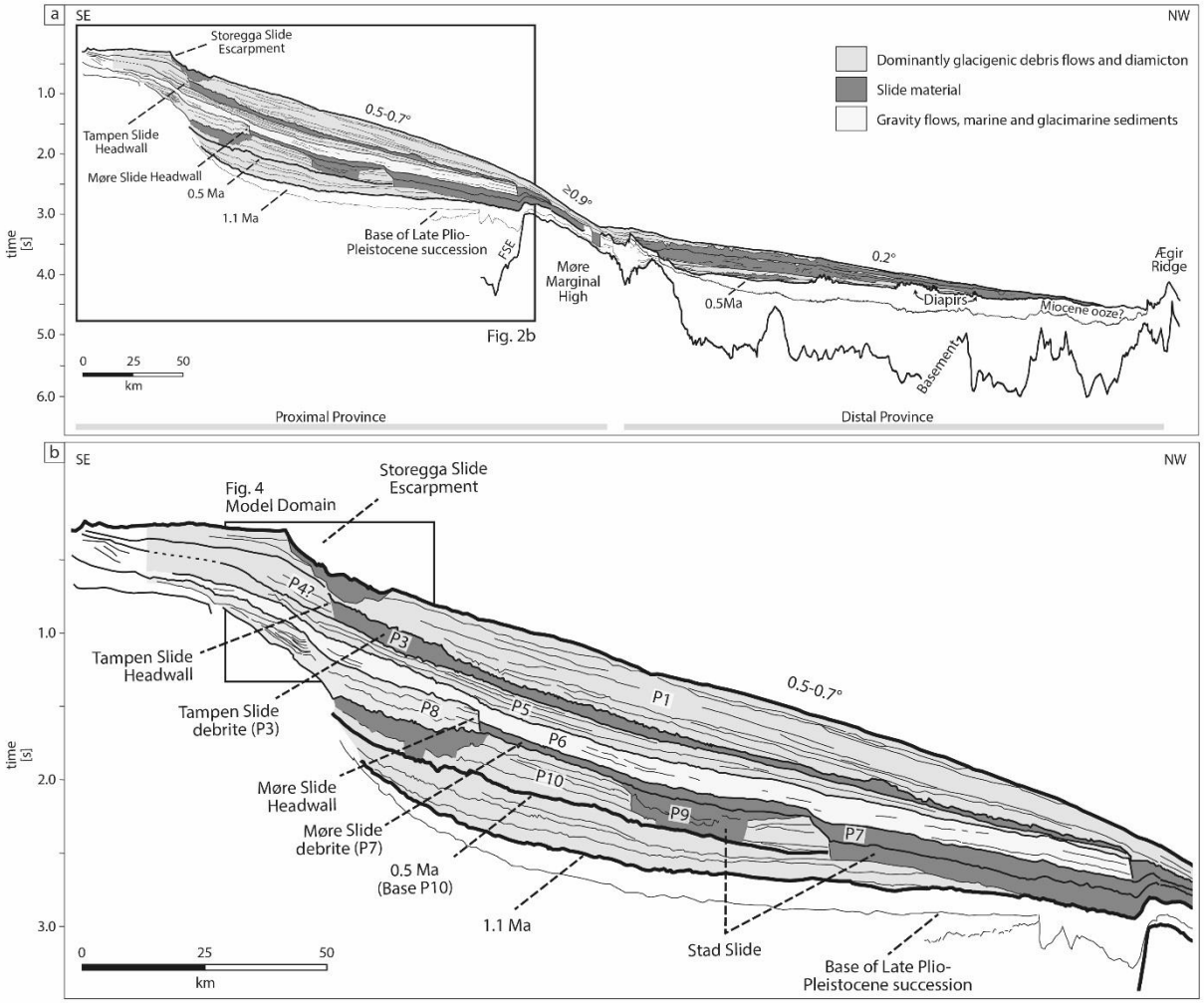

Fig. 2. a) Interpreted seismic profile across the North Sea TMF (modified after Nygård et al., 2005 and Hjelstuen et al., 2012). Seismostratigraphic units (P1-P10) and identified time horizons are indicated. Profile location in Fig. 1. FSE: Faroe-Shetland Escarpment, **b)** Blow-up of the proximal province of the North Sea TMF.

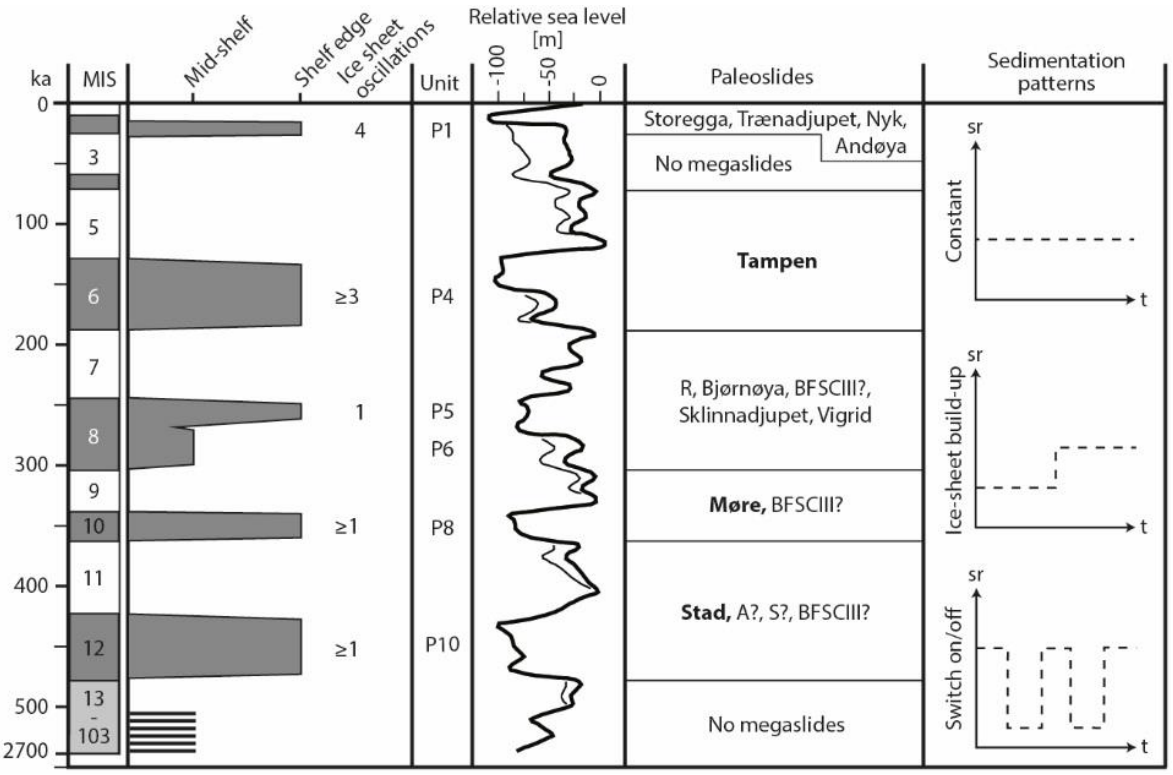

Fig. 3. Assumed shelf edge glaciations of the Norwegian Channel Ice Stream during the past 500 ka (modified after Nygård et al., 2005). Seismic units (P1-P10), relative sea level curve (Skene et al., 1998), paleoslides identified along the Norwegian-Barents Sea margin (summarized by Hjelstuen et al., 2007) and sedimentation patterns used in the different model runs of this study are shown. Slides on the North Sea TMF are indicated in bold. Shelf-edge glaciations dominate the late Quaternary sedimentation, whereas a different ice-sheet configuration is documented in early and mid-Quaternary (Batchelor et al., 2017). MIS: Marine isotope stage, sr: Sedimentation rate, t: Time.

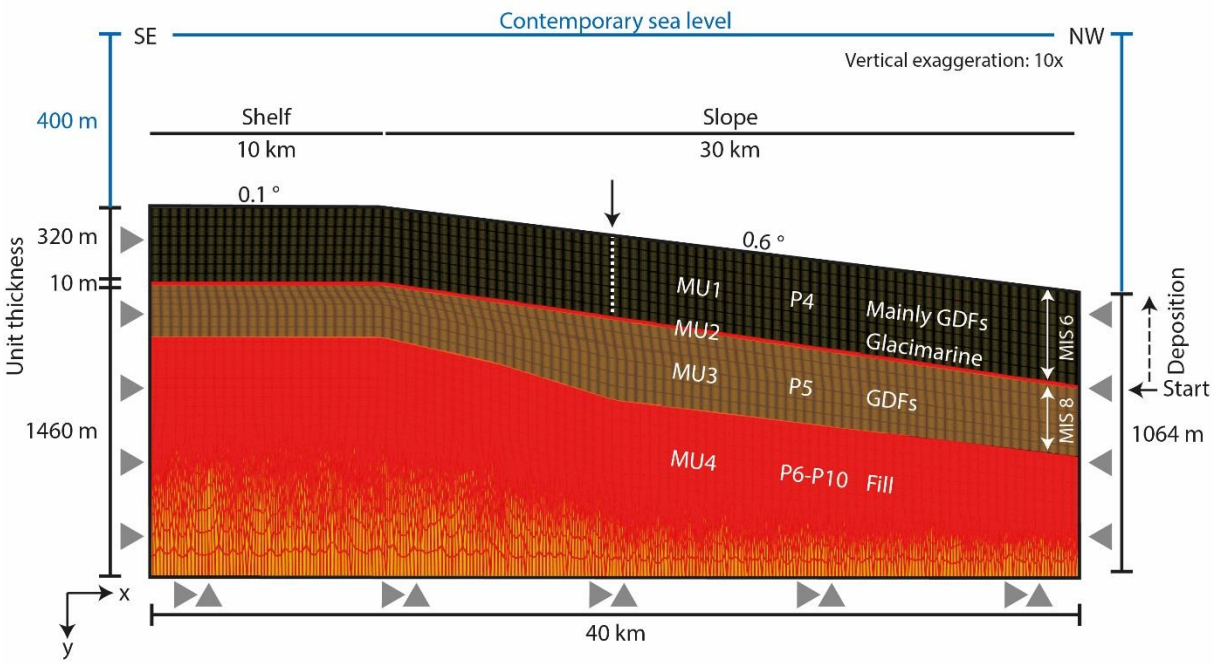

Fig. 4. Two-dimensional model geometry for the time of the Tampen Slide (130 ka BP) reconstructed based on the identified seismic sequences P4-P10 of Nygård et al. (2005). Headwall of the Tampen Slide (white stippled line) and thin glacimarine layer (red line) are shown. Black arrow indicates location of the profiles for the model output parameters (Figs. 7-9). Triangles indicate displacement boundary conditions. The model simulations start with the deposition of eight rows of MU1. GDF: Glacigenic debris flow. MU: Model unit.

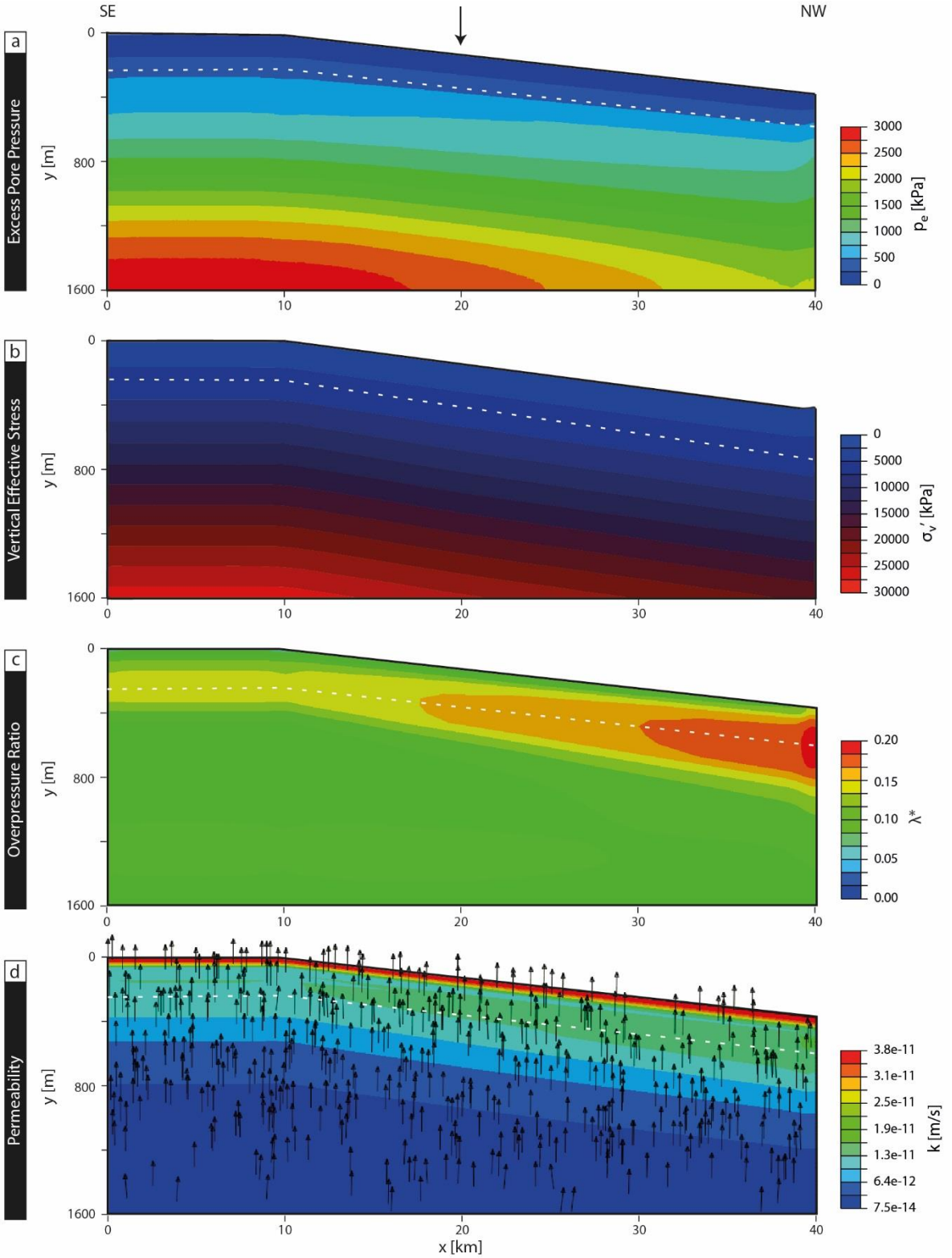

Fig. 5. Results of 2D FE consolidation analysis for the reference model run after deposition of MU1. White stippled line indicates location of glacimarine layer (MU2) and black arrow show the position of the Tampen Slide headwall. Note a vertical exaggeration of 10. Vectors in the permeability plot are randomly selected, and only show the direction of fluid flow, but not the magnitude.

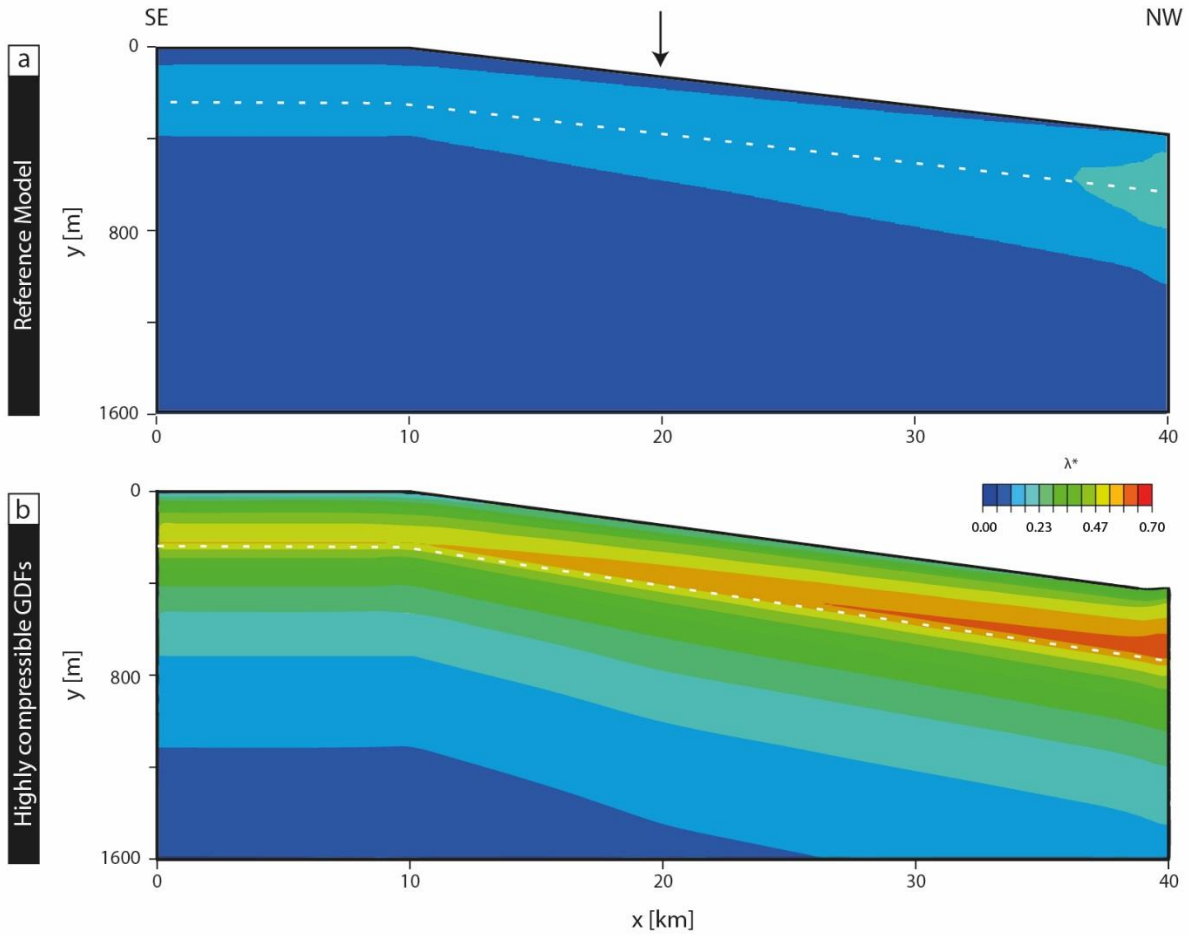

1032

1033 **Fig. 6.** Comparison of overpressure ratio for different compressibilities (λ) in MU1 at the end of MIS 6.

1034 **a)** Reference model with λ = 0.10, **b)** Reference model with λ = 0.13.

1035

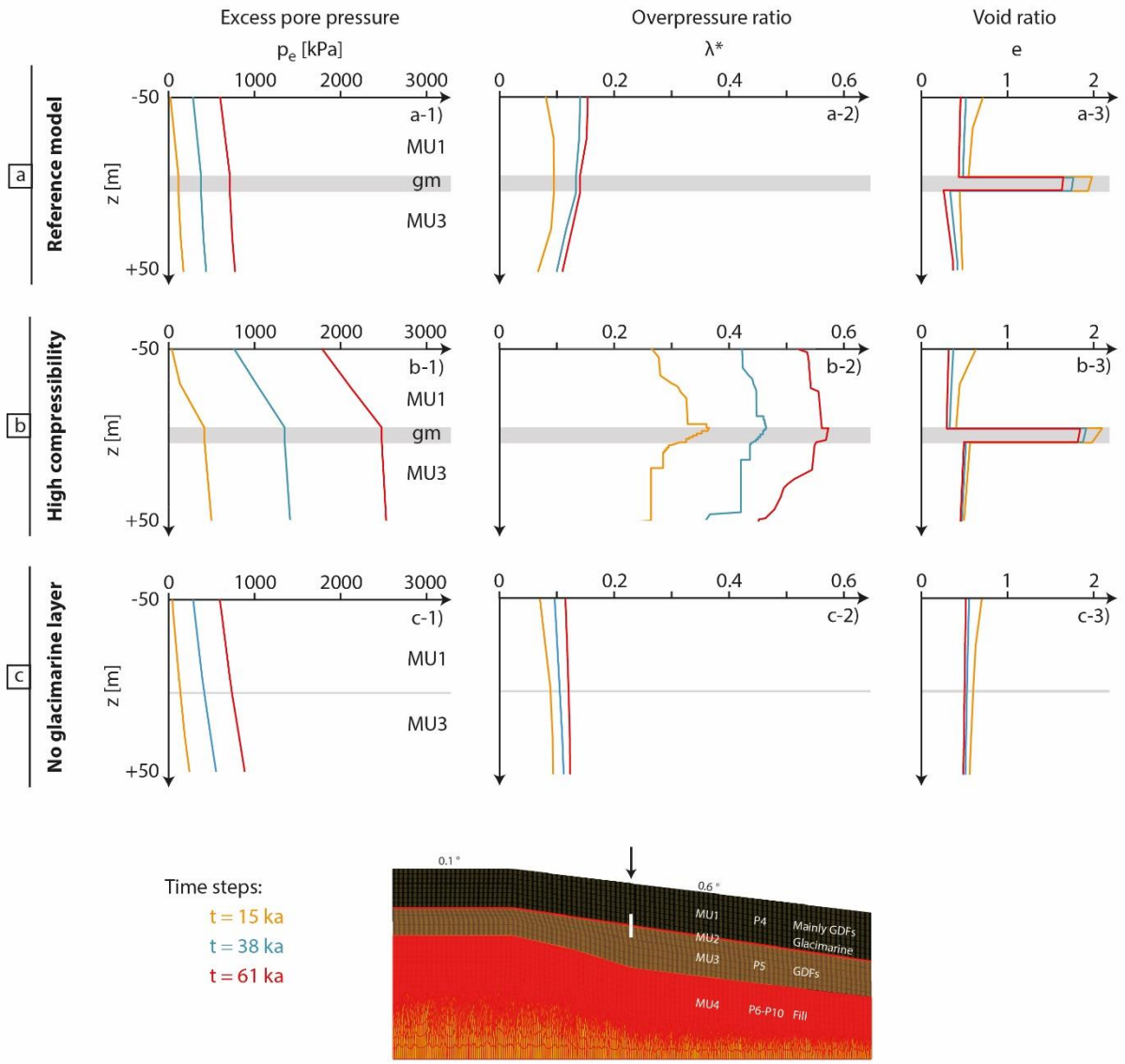

Fig. 7. Vertical profiles visualizing the effect of the glacimarine layer on slope stability. Vertical profiles ±50m of the glacimarine layer at x = 20 km (white bar) are shown for several simulation time steps represented by different colors. Color coding as well as location of vertical profiles in the model domain are given at the bottom of the figure. The profiles show the evolution in time of excess pore pressure (p_e), overpressure ratio (λ*) and void ratio (e).

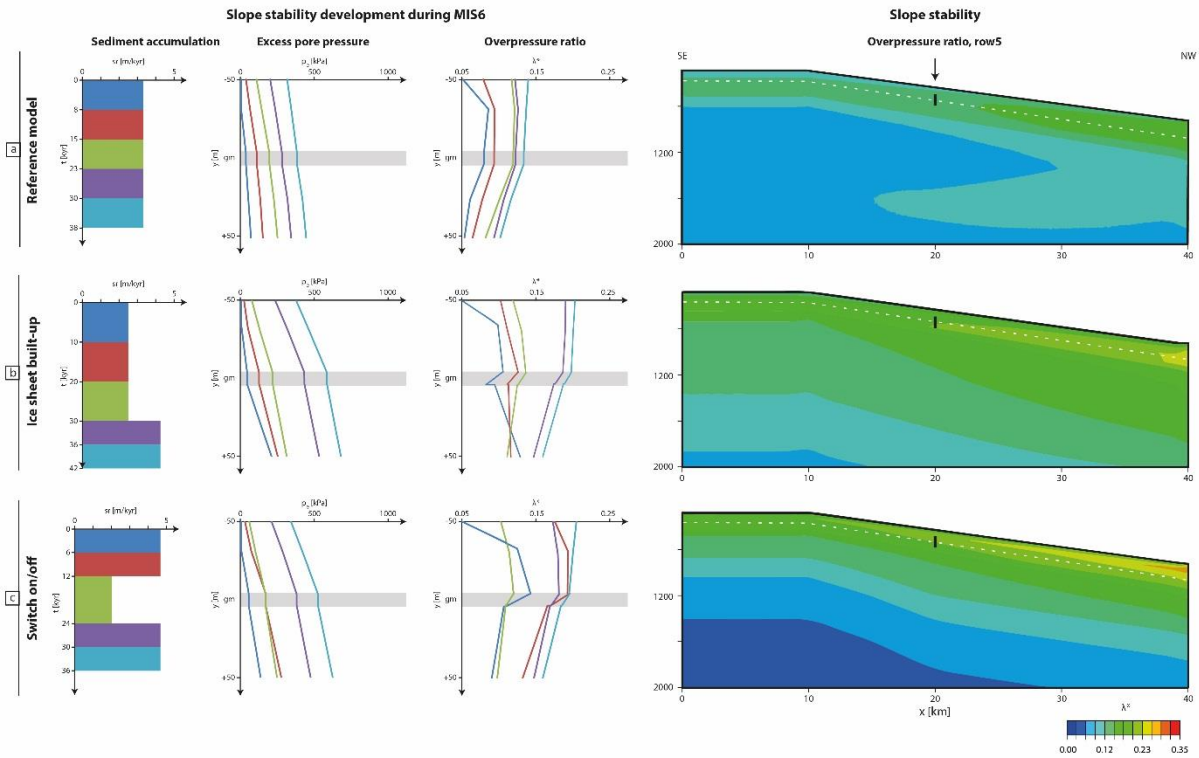

1043

1044 **Fig. 8.** Vertical profiles ± 50m of the glacimarine layer for the three sedimentation patterns showing the
1045 evolution in time (different colors representing different time steps) of excess pore pressure (p_e) and
1046 overpressure ratio (λ*). Results of 2D FE consolidation analysis are shown to the right. **a)** Model run
1047 with constant sediment load, **b)** Model run with variable sediment load, **c)** Model run with episodic
1048 sediment load.

1049

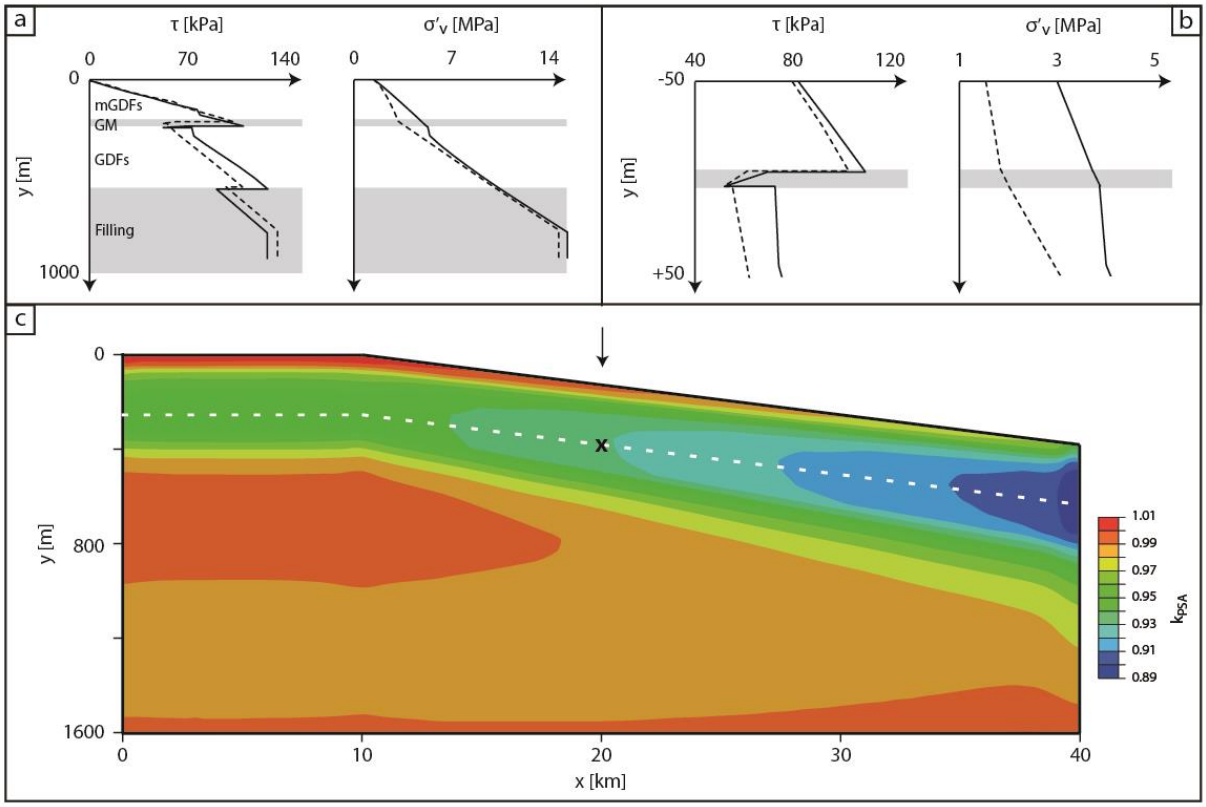

Fig. 9. a) Vertical profiles for shear stress τ and vertical effective stress σ'_v. We assume that the slope will fail at the depth with highest shear stresses and lowest vertical effective stresses, which correlates with the glacimarine layer (GM). Results of the reference model with measured compressibilities (black line) and high-compressible layer mainly consisting of GDFs (stippled line) are indicated. **b)** Blow-up along the expected location of slope failure. **c)** Peak spectral acceleration (k_{PSA}) of the 2D FE consolidation analysis for the reference model run with measured sediment properties at the age of the Tampen Slide (t = 130 ka BP). White stippled line indicates location of glacimarine layer (MU2), black arrow show the position of Tampen Slide headwall and the black cross the expected point of slope failure.

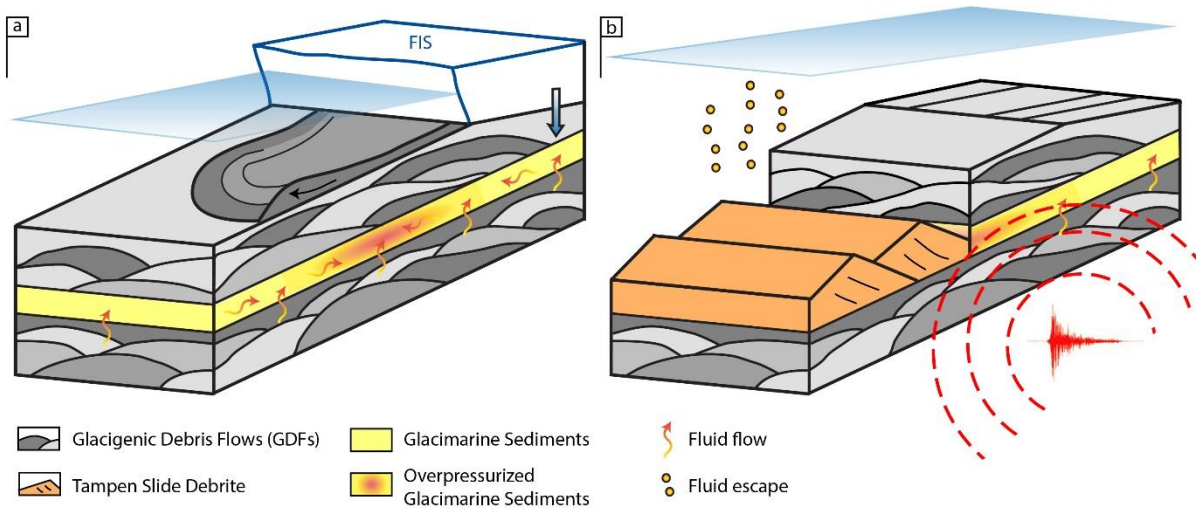

Fig. 10. Conceptual sketch showing preconditioning and triggering of the Tampen Slide. **a)** Glacigenic debris flows are common sedimentary processes during the MIS 6 shelf edge glaciations of the Fennoscandian Ice Sheet (FIS). Numerous sequences of stacked and rapidly-deposited glacigenic debris flows act as a seal for vertical fluid flow, and fluids accumulate in the glacimarine layer. The highest overpressure ratios are generated c. 10 km away from the shelf edge, where the sediment accumulation is highest. **b)** A earthquake of M6.9 or larger at a short distance from the Tampen Slide headwall trigger the Tampen Slide at the location where highest overpressure values have been generated. The glacimarine layer can only be identified upslope of the Tampen Slide headwall, where it still might be overpressured.

Tab. 1. Model Units (MU) of this study. Thicknesses, P-wave velocities and ages according to Nygård et al. (2005). Thicknesses in ms as observed in seismic profiles; thicknesses in m inferred from P-wave velocities; CSU: Corresponding seismic unit after Nygård et al. (2005), GDFs: Glacigenic debris flows, GMs: Glacimarine sediments, GFs: Gravity flows, MIS: Marine isotope stage, x: undefined.

MU	CSU	Sediment type	Thickness [ms]	Thickness [m]	P-wave [m/s]	Time [ka]	Age	Relative sedimentation
1+2	P4	Mainly GDFs	259	246	1900	113	MIS 6	High
1	P4	Mainly GDFs	x	236	x	61	MIS 6	High
2	P4	GMs/GFs	x	10	x	52	MIS 7-8	Moderate
3	P5	GDFs	74	63	1900	57	MIS 8	High
4	P6-P10	Fill	x	x	x	178	MIS 9-12	Low-High

Tab. 2. Sediment properties of the material used in the modeling. Geotechnical correlations established by NGI (Kvalstad et al., 2005a).

	Glacial debris	Mainly glacial debris	(Glaci)-marine sediments
Poisson ratio, ν	0.3	0.3	0.3
Friction angle, φ [°]	28	28	28
Dry density, ρ_{dry} [kg/m^3]	2.0	2.0	1.8
Void ratio, e0	1.2	1.2	3.5
Compressibility*, λ	0.04-0.17 (e → 0.08-1.2)	0.1	0.13-0.57 (e → 0.25-2.77)
Corresponding seismic unit	P5	P4	Layer between P4 and P5

*Logarithmic bulk modulus; void-ratio dependent

Tab. 3. Model scenarios. Compressibility (λ), permeability (k) and void ratio (e) defined in Tab. 3. A: 3.3 m/ka, B: 2.5 m/ka, C: 4.2 m/ka, D: 2.1 m/ka. GM: Glacimarine sediments, GDFs: Glacigenic debris flows, MGDF: Mainly glacigenic debris flows, k_x: Horizontal permeability, k_y: Vertical permeability. Consolidation properties based on geotechnical analyses of sediments from the Ormen Lange area (NGI, Kvalstad et al., 2005b).

	Time [ka]	Sedimentation rate	λ_{GM}	λ_{GDF}	λ_{MGDF}	k_x/k_y
Reference Model	61	A	Tab. 2	Tab. 2	0.1	1
Reference Model, high compressibility	61	A	Tab. 2	Tab. 2	0.13	1
Reference Model, no glacimarine layer	61	A	Tab. 2	Tab. 2	0.1	1
Reference Model, 5 rows	38	A	Tab. 2	Tab. 2	0.1	1
Ice-sheet built-up, 5 rows	42	B/C	Tab. 2	Tab. 2	0.1	1
Switch on/off, 5 rows	36	C/D/C	Tab. 2	Tab. 2	0.1	1